Effect of control parameters on biogas production during the anaerobic digestion of protein-rich substrates

Z. Khedim, Boumédiène Benyahia, Brahim Cherki, Tewfik Sari, Jérôme Harmand

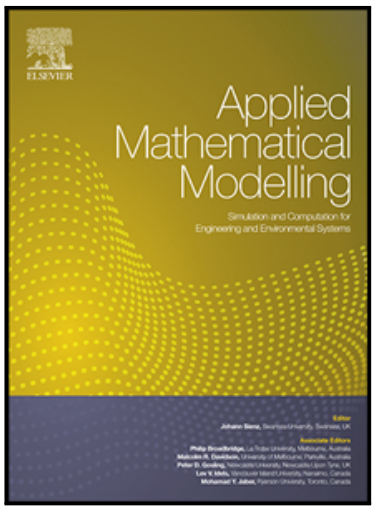

Effect of control parameters on biogas production during the anaerobic digestion of protein-rich substrates

Zeyneb Khedim, Boumediène Benyahia, Brahim Cherki, Tewfik Sari, Jérôme Harmand

PII: S0307-904X(18)30205-1
DOI: 10.1016/j.apm.2018.04.020
Reference: APM 12259

To appear in: *Applied Mathematical Modelling*

Received date: 8 September 2017
Revised date: 13 February 2018
Accepted date: 25 April 2018

Please cite this article as: Zeyneb Khedim, Boumediène Benyahia, Brahim Cherki, Tewfik Sari, Jérôme Harmand, Effect of control parameters on biogas production during the anaerobic digestion of protein-rich substrates, *Applied Mathematical Modelling* (2018), doi: 10.1016/j.apm.2018.04.020

Highlights

- A model of Anaerobic Digestion of protein-rich Microalgae (MAD) was analyzed
- An insight on the process behavior as a function of control parameters was provided
- Operating Diagram defined the ideal conditions to optimize biogas yield and ammonia toxicity
- Application of MAD model is limited in acidic environments
- Qualitative-quantitative properties of ADM1m model were derived from those of MAD

Effect of control parameters on biogas production during the anaerobic digestion of protein-rich substrates

Zeyneb Khedim[a,*], Boumediène Benyahia[a], Brahim Cherki[a], Tewfik Sari[b], Jérôme Harmand[c]

[a] *Laboratoire d'Automatique de Tlemcen, Université de Tlemcen. BP 230 Tlemcen 13000, Algeria*
[b] *Irstea, UMR ITAP, Univ Montpellier, 34196, Montpellier, France*
[c] *LBE, INRA, Univ Montpellier,* 11100*, Narbonne, France*

Abstract

This paper deals with the theoretical study of the anaerobic digestion of protein-rich substrates. Since the success of such digestion raises the issue of the possible release of ammonia, we have carried out a mathematical analysis of an Anaerobic Digestion model specifically developed for the treatment of Microalgae, termed MAD (Microalgae Anaerobic Digestion) in the literature. Our aim is to investigate the qualitative properties of the system via the calculation of its equilibria, their conditions of existence as well as their stability according to the operating parameters values. Simulation results highlight the key parameters acting on model behavior. In particular, it is shown that the control parameters can greatly affect biogas yield and, thus, process performance. The optimal conditions for process operation are then identified. To emphasize the effect of pH on biological reactions, we plot the operating diagram of the MAD model for different fixed pH values. We demonstrate that a rising pH favors the formation of the free ammonia, leading ultimately to methanogen inhibition. Surprisingly, our study highlights the insensitivity of the model to acidic environments, thus limiting its potential applications at low pH. Finally, we investigate the qualitative and quantitative properties of a modified ADM1 (Anaerobic Digestion Model n^{o}1) model in the light of those of the MAD model.

Keywords: Anaerobic Digestion, equilibria, model, Microalgae, operating diagram, stability analysis

*Corresponding author
Email addresses: zeyneb.khedim@univ-tlemcen.dz (Zeyneb Khedim), b.benyahia.ut1@gmail.com (Boumediène Benyahia), b.cherki@gmail.com (Brahim Cherki), tewfik.sari@irstea.fr (Tewfik Sari), jerome.harmand@inra.fr (Jérôme Harmand)

1. Introduction

Anaerobic Digestion (AD) is a biological process, which reduces organic pollution and produces renewable energy (biogas). This kind of bioprocess is regarded as an alternative energy source to fossil fuel.
In order to maximize its efficiency, anaerobic digestion is now widely used at full-scale to degrade various organic feedstocks. Special Attention has been paid to the fermentation of protein-rich substrates, in view of their outstanding yield of biogas and fertilizers [1], [2].

However, despite its energetic benefit, the fermentation of such substrates leads to high concentrations of nitrogen in the reaction medium derived from the breakdown of protein. Nitrogen is converted into ammonium (NH_4^+) and free ammonia NH_3, which is toxic for bacterial communities at high concentrations. Ammonia toxicity can cause serious problems of instability leading to dramatic damage of the process and even its failure.

Environmental factors such as temperature, pH, bacterial acclimation, can have a significant effect on such phenomena. Furthermore, control parameters as the dilution rate or the feed concentration at inlet might significantly influence the whole process performances [3].

Many researches were established to assess operating conditions impact on nitrogen inhibition. In this context, ammonia influence on AD has been evaluated at a mesophilic temperature [4]. Its threshold level for inhibition has been ascertained for the anaerobic digestion of saline wastewater [5], while the impact of its concentration and of Hydraulic Retention Time (HRT) has been studied in [6].
To deal with such an inhibition in practice, alternative solutions have been also suggested either by: i) the addition of certain elements to the feed substrate (co-digestion of meat and kitchen waste to extend the C:N ratio [2] and adding trace elements throughout the Anaerobic Digestion of food wastes [7]); or by ii) keeping the factors limiting ammonia inhibition at their optimum values in testing the impact of Organic Loading Rate (OLR) and Hydraulic Retention Time (HRT) on the AD of animal byproducts [8], and investigate pH impact on the AD of kitchen waste [9].

In addition, some experimental applications has been focused on the optimization of protein-rich substrates digestion. The OLR was optimized under different temperatures throughout the digestion of slaughterhouse waste [10]. The useful agents for maximizing biogas generation from the AD of slaughterhouse by-products (blood, meat, ribs, fat, raw waste) were studied in [11], while the efficacy of co-digestion of gelatin and turkey was addressed in [12].

Elsewhere, other studies have modeled the digestion of protein-rich substrates such as the models proposed by Batstone et al. [13] and Lokshina et al.[14], developed to describe the AD of slaughterhouse wastewater. Besides, Angelidaki et al. were interested in the validation of an existing model of AD using experimental data of the co-digestion of manure and protein-rich wastewater [15].
In [16], the AD of *chlorella vulgaris* microalgae was considered, in terms of composition, as a source of proteins. A model for Microalgae AD (hereafter denoted as the "MAD model") were proposed. It was validated on experimental data and compared to a modified ADM1 model specifically adapted to the digestion of microalgae [17].

Most previous studies used experimental results of various substrates digestion to derive ideal values for operating parameters, while our present contribution is to emphasize [17] in simulation the influence of these parameters on the qualitative behavior of the process. To do so, we investigate the properties of the MAD model and we compare them to those of ADM1

In this paper, we focus on the mathematical study of the MAD model in order to identify ideal conditions of the process operation. An exhaustive analysis of its equilibria, their stability and their bifurcation properties was established. Subsequently, process performance was evaluated in terms of biogas production in order to define the optimal ranges of pH, dilution rate (D), organic load (S_{in}) and inorganic nitrogen concentration (N_{in}), which ensuring maximum yield from fermentation. Based on the present study, we show how control parameters affect system performance. In particular, the favorable conditions for ideal biogas production have been stressed.
The paper is organized as follows: first, the MAD model is presented and its equilibria are calculated. Stability of equilibria is evaluated with respect of control parameters changes. Thereafter, the Operating Diagrams (OD) of the system are presented under different degrees of acidity to investigate the effect of pH on the anaerobic digestion. In addition, the process performance is assessed by following the evolution of biogas production. Simulation results highlight the effect of control parameters on the digestion and validate the improved theoretical analysis. Finally, discussions and general conclusions are drawn.

2. Mathematical analysis of Microalgae Anaerobic Digestion model

2.1. Presentation of MAD model

We consider here the three reaction-two step model of Microalgae Anaerobic Digestion (MAD) proposed by Mairet et al. [16]. The model involves four sub-

strates (S_1 sugars/lipids, S_2 proteins, S_3 VFAs[1] and S_I inerts), and three bacterial groups (X_1 sugar/lipid-degrading bacteria, X_2 protein-degrading bacteria and X_3 VFA-degrading methanogens), (see Figure 1). Mathematical equations of the MAD model are given by:

$$\begin{aligned}
\dot{S}_1 &= D\left(\beta_1 S_{in} - S_1\right) - \alpha_1\mu_1 X_1 && (1)\\
\dot{S}_2 &= D\left(\beta_2 S_{in} - S_2\right) - \alpha_5\mu_2 X_2 && (2)\\
\dot{S}_3 &= -DS_3 + \alpha_3\mu_1 X_1 + \alpha_6\mu_2 X_2 - \alpha_9\mu_3 X_3 && (3)\\
\dot{X}_1 &= \left(\mu_1 - D\right) X_1 && (4)\\
\dot{X}_2 &= \left(\mu_2 - D\right) X_2 && (5)\\
\dot{X}_3 &= \left(\mu_3 - D\right) X_3 && (6)\\
\dot{N} &= D\left(N_{in} - N\right) - \alpha_2\mu_1 X_1 + \alpha_7\mu_2 X_2 - \alpha_{10}\mu_3 X_3 && (7)\\
\dot{C} &= D\left(C_{in} - C\right) + \alpha_4\mu_1 X_1 + \alpha_8\mu_2 X_2 + \alpha_{12}\mu_3 X_3 - \rho_{CO_2} && (8)\\
\dot{P}_{CO_2} &= -P_{CO_2}\frac{q_{gas}}{V_{gas}} + \rho_{CO_2}\frac{V_{liq}RT_{op}}{V_{gas}} && (9)\\
\dot{P}_{CH_4} &= -P_{CH_4}\frac{q_{gas}}{V_{gas}} + \rho_{CH_4}\frac{V_{liq}RT_{op}}{V_{gas}} && (10)\\
\dot{z} &= D\left(z_{in} - z\right) && (11)\\
\dot{S}_I &= D\left(\beta_I S_{in} - S_I\right) && (12)
\end{aligned}$$

where D is the dilution rate, $\alpha_i (i = 1, ..., 12)$ are the stoichiometric parameters, $\beta_i (i = 1, 2, I)$ are the fractionation coefficients, S_{in}, N_{in}, C_{in} and z_{in} denote, respectively, inlet concentrations of the organic matter, the inorganic nitrogen N, the inorganic carbon C and the alkalinity z.
P_{CO_2} and P_{CH_4} are the partial pressures of the CO_2 and CH_4 while ρ_{CO_2} and ρ_{CH_4} are their liquid-gas transfer rates defined as:

$$\rho_{CO_2} = k_L a\left(\frac{h}{K_C + h}C - K_{H,CO2}P_{CO2}\right) \quad (13)$$

$$\rho_{CH_4} = \alpha_{11}\mu_3 X_3 \quad (14)$$

$$q_{gas} = k_p\left(P_{CH_4} + P_{CO_2} - P_{atm}\right) \quad (15)$$

[1] Volatile Fatty Acid

V_{liq}, V_{gas}, R, k_La, T_{op}, P_{atm}, q_{gas}, k_p, h denote, respectively, the liquid volume, gas volume, gas law constant, physico-chemical coefficient, temperature, atmospheric pressure, gas flow, pipe resistance coefficient and the concentration of the hydrogen/hydroxide ions. K_C and $K_{H,CO2}$ are, respectively, chemical constants of dissociation and of volatility (Henry's law).
The kinetics μ_1 and μ_2 are ratio-dependent functions: they depend on S_i/X_i $(i = 1, 2)$. Such functions are represented by the Contois model:

$$\mu_i(S_i, X_i) = \bar{\mu}_i \frac{S_i}{(S_i + K_{Si}X_i)}, i = (1, 2) \tag{16}$$

where $\bar{\mu}_i$ $(i = 1, 2)$ are the maximum specific growth rates of the bacteria X_i, K_{Si} is the Contois half saturation constants.
The kinetic μ_3 depends on both S_3 and NH_3. It is modeled by the following function:

$$\mu_3(S_3, NH_3) = \bar{\mu}_3 \frac{S_3}{S_3 + K_{S_3} + \frac{S_3^2}{K_{I3}}} \frac{K_{I,nh_3}}{K_{I,nh_3} + NH_3} \tag{17}$$

with $\bar{\mu}_3$ the maximum specific growth rate of the bacteria X_3, K_{S3} is the Haldane half saturation constant, K_{I3} is the Haldane inhibition constant and K_{I,nh_3} is the ammonia inhibition constant.

The association or dissociation of total inorganic nitrogen N with hydrogen/hydroxide ions determine the formation of ammonia NH_3 and ammonium NH_4^+. At equilibrium, this physico-chemical process is characterized by a dissociation constant K_N defined as: $K_N = h[NH_3]/[NH_4^+]$. Thus, μ_3 can be written as:

$$\mu_3(S_3, N) = \bar{\mu}_3 \frac{S_3}{S_3 + K_{S_3} + \frac{{S_3}^2}{K_{I3}}} \frac{K_{I,nh_3}}{K_{I,nh_3} + \lambda N}, \quad \lambda = \frac{K_N}{K_N + h} \tag{18}$$

In view of low values of HRT adopted in the experiments of Mairet et al. [16], bacterial decay rate was not taken into account in the model's equations.

Hypothesis. $pH = -log_{10}[h]$ constant, which implies that λ is constant.

For simplicity, we overlook in the mathematical analysis the equations (8), (9) and (10), which are model outputs. The equations (11) and (12) are also ignored due to the assumption that the pH is constant.
Hence, we consider the reduced model (1)-(7) and we denote $\xi = [S_1, S_2, S_3, X_1, X_2, X_3, N]^T$ the state vector.

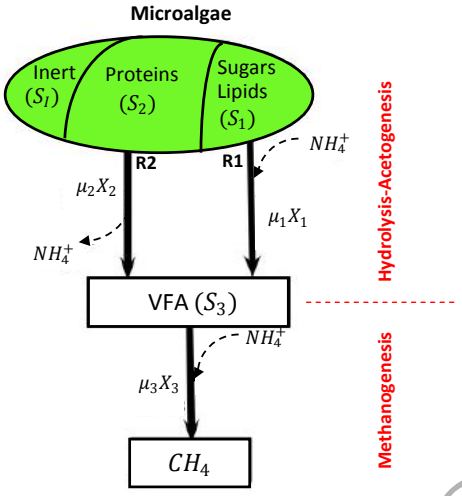

Figure 1: Reaction stages considered in the MAD model [16].

2.2. Equilibria of the model

The equilibria of the reduced MAD model are given by the solutions of the following system of algebraic equations:

$$\begin{cases} 0 = D(\beta_1 S_{in} - S_1) - \alpha_1 \mu_1 X_1 & \text{(19a)} \\ 0 = D(\beta_2 S_{in} - S_2) - \alpha_5 \mu_2 X_2 & \text{(19b)} \\ 0 = -DS_3 + \alpha_3 \mu_1 X_1 + \alpha_6 \mu_2 X_2 - \alpha_9 \mu_3 X_3 & \text{(19c)} \\ 0 = (\mu_1 - D) X_1 & \text{(19d)} \\ 0 = (\mu_2 - D) X_2 & \text{(19e)} \\ 0 = (\mu_3 - D) X_3 & \text{(19f)} \\ 0 = D(N_{in} - N) - \alpha_2 \mu_1 X_1 + \alpha_7 \mu_2 X_2 - \alpha_{10} \mu_3 X_3 & \text{(19g)} \end{cases}$$

Eight cases are considered, which are reported in Table 1.

Table 1: Different cases for equilibria

Case1	$X_1 = 0$	$X_2 = 0$	$X_3 = 0$
Case2	$X_1 = 0$	$\mu_2(S_2, X_2) = D$	$X_3 = 0$
Case3	$X_1 = 0$	$\mu_2(S_2, X_2) = D$	$\mu_3(S_3, N) = D$
Case4	$\mu_1(S_1, X_1) = D$	$X_2 = 0$	$X_3 = 0$
Case5	$\mu_1(S_1, X_1) = D$	$X_2 = 0$	$\mu_3(S_3, N) = D$
Case6	$\mu_1(S_1, X_1) = D$	$\mu_2(S_2, X_2) = D$	$X_3 = 0$
Case7	$\mu_1(S_1, X_1) = D$	$\mu_2(S_2, X_2) = D$	$\mu_3(S_3, N) = D$
Case8	$X_1 = 0$	$X_2 = 0$	$\mu_3(S_3, N) = D$

calculation.

Due to the absence of the inlet concentration S_{3in} of Volatile Fatty Acid in the model, case 8 is biologically impossible and thus it will be not taken into account. Hence, the equations (19a, 19d), (19b, 19e), (19c, 19f and 19g) can be solved considering the following three subsystems of equations:

$$\begin{cases} \bar{\mu}_1 \dfrac{S_1}{S_1 + K_{S_1} X_1} = \mathrm{D} & (20a) \\ S_1 + \alpha_1 X_1 = \beta_1 S_{in} & (20b) \end{cases}$$

$$\begin{cases} \bar{\mu}_2 \dfrac{S_2}{S_2 + K_{S_2} X_2} = \mathrm{D} & (21a) \\ S_2 + \alpha_5 X_2 = \beta_2 S_{in} & (21b) \end{cases}$$

$$\begin{cases} -S_3 + \alpha_6 X_2 + \alpha_3 X_1 - \alpha_9 X_3 = 0 & (22a) \\ N_{in} - N - \alpha_2 X_1 + \alpha_7 X_2 - \alpha_{10} X_3 = 0 & (22b) \\ \bar{\mu}_3 \dfrac{S_3}{S_3 + K_{S_3} + \frac{{S_3}^2}{K_{I3}}} \dfrac{K_{I,nh_3}}{K_{I,nh_3} + \lambda N} = D & (22c) \end{cases}$$

From the equation (20a), we have:

$$S_1^* = \frac{D K_{S_1} X_1^*}{\bar{\mu}_1 - D} \tag{23}$$

which is non-negative if, and only if, $\bar{\mu}_1 - D > 0$.

By combining equations (20a) and (20b), we have:

$$X_1^* = \frac{\beta_1 S_{in}}{\frac{D K_{S_1}}{\bar{\mu}_1 - D} + \alpha_1} \tag{24}$$

Combining this expression with (23), we obtain:

$$S_1^* = \beta_1 S_{in} \frac{DK_{S_1}}{DK_{S_1} + \alpha_1(\bar{\mu}_1 - D)} \tag{25}$$

Thus, if S_1^* exists *i.e.* if $D < \bar{\mu}_1$, then S_1^* is necessarily smaller than $\beta_1 S_{in}$. From equation (21a) we calculate:

$$S_2^* = \frac{DK_{S_2} X_2^*}{\bar{\mu}_2 - D} \tag{26}$$

which is non-negative if, and only if, $\bar{\mu}_2 - D > 0$.

Combining equations (21a) and (21b) we have:

$$X_2^* = \frac{\beta_2 S_{in}}{\frac{DK_{S_2}}{\bar{\mu}_2 - D} + \alpha_5} \tag{27}$$

Combining the last expression with (26), we obtain:

$$S_2^* = \beta_2 S_{in} \frac{DK_{S_2}}{DK_{S_2} + \alpha_5(\bar{\mu}_2 - D)} \tag{28}$$

Thus, if S_2^* exists *i.e.* if $D < \bar{\mu}_2$, then S_2^* is necessarily smaller than $\beta_2 S_{in}$. From (22a), we get:

$$X_3^* = \frac{1}{\alpha_9}(S_{3in}^* - S_3^*) \tag{29}$$

Equation (22b) gives:

$$N^* = N_{in}^* - \alpha_{10} X_3^* \tag{30}$$

with

$$S_{3in}^* = \begin{cases} S_{3in,1}^* = \alpha_3 X_1^* & \text{if only the reaction1 (R1) occurs (Figure 1)} \\ S_{3in,2}^* = \alpha_6 X_2^* & \text{if only the reaction2 (R2) occurs (Figure 1)} \\ S_{3in,total}^* = \alpha_3 X_1^* + \alpha_6 X_2^* & \text{if both reactions (R1) and (R2) occur (Figure 1)} \end{cases}$$

$$N_{in}^* = \begin{cases} N_{in,1}^* = N_{in} - \alpha_2 X_1^* & \text{if only the reaction1 (R1) occurs (Figure 1)} \\ N_{in,2}^* = N_{in} + \alpha_7 X_2^* & \text{if the only reaction2 (R2) occurs (Figure 1)} \\ N_{in,total}^* = N_{in} - \alpha_2 X_1^* + \alpha_7 X_2^* & \text{if both reactions (R1) and (R2) occur (Figure 1)} \end{cases}$$

Figure 2 illustrates the cascade structure of the system leading to different concentrations of S_{3in}^* and N_{in}^*.

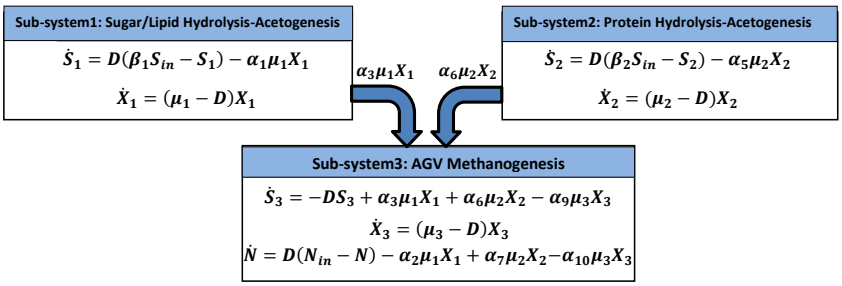

Figure 2: The structure of the system.

From (29) and (30), we deduce that

$$N^* = A + \frac{\alpha_{10}}{\alpha_9} S_3^*, \quad \text{where } A := N_{in}^* - \frac{\alpha_{10}}{\alpha_9} S_{3in}^* \tag{31}$$

Replacing this expression in (22c), we find that S_3^* is the solution of the following equation:

$$\bar{\mu}_3 \frac{S_3}{S_3 + K_{S_3} + \frac{{S_3}^2}{K_{I3}}} = D \frac{K_{I,nh_3} + \lambda\left(A + \frac{\alpha_{10}}{\alpha_9} S_3\right)}{K_{I,nh_3}}$$

Thus, S_3 is the intersection of a Haldane function $f(S_3)$ with a rising line $g(S_3)$ defined as:

$$f(S_3) = \bar{\mu}_3 \frac{S_3}{S_3 + K_{S_3} + \frac{{S_3}^2}{K_{I3}}}$$

$$g(S_3) = D \frac{K_{I,nh_3} + \lambda\left(A + \frac{\alpha_{10}}{\alpha_9} S_3\right)}{K_{I,nh_3}}$$

Hence, we can obtain 2, 1 or 0 intersection(s). There are, thus, at most only two positive equilibria. This is schematically represented in Figure 3.

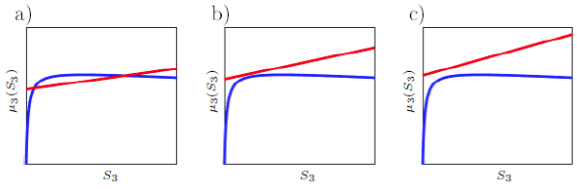

Figure 3: Possible cases of the intersection of functions $f(S_3)$ (blue lines), $g(S_3)$ (red lines), a) Two intersections, b) One intersection, c) No intersection.

From equation (29), we can see that S_3^* is accepted if, and only if, $S_3^* < S_{3in}^*$, because X_3^* should be positive. Thus, the condition $f(S_{3in}^*) = g(S_{3in}^*)$ is crucial for evaluating if the solutions S_3^* are accepted or not.
According to the sign of the equation $f(S_{3in}^*) - g(S_{3in}^*)$, we can investigate the values of S_3^* with respect to those of S_{3in}^*. In the case of two intersection (Figure 3-a), we can deduce the sub-cases illustrated in Figure 4.

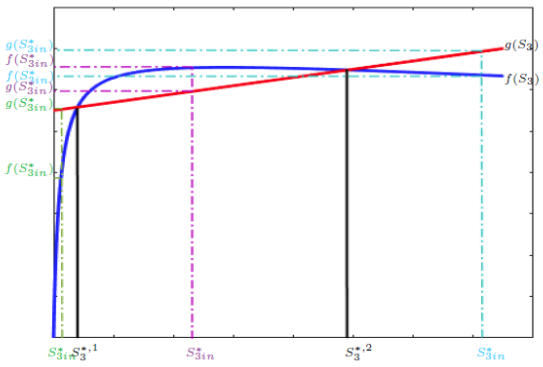

Figure 4: Possible positions of S_{3in}^* in relation to $S_3^{*1}$and S_3^{*2}.

When $f(S_{3in}^*) - g(S_{3in}^*) < 0$, we have i) no solution if $S_{3in}^* < S_3^{*,1} < S_3^{*,2}$ (Figure 4, green dashed lines); or ii) two solutions $S_3^{*,1} > 0$ and $S_3^{*,2} > 0$ if $S_3^{*,1} < S_3^{*,2} < S_{3in}^*$ (Figure 4, cyan dashed lines).
If $f(S_{3in}^*) - g(S_{3in}^*) > 0$, only one solution is accepted: $S_3^{*,1} > 0$ (Figure 4, magenta dashed lines). The solution $S_3^{*,2} > S_{3in}^*$ gives $X_3^{*,2} < 0$ according to (29).
Substituting the feasible solutions $S_3^{*,i}$ in the equation (29), we deduce $X_3^{*,i}$ $(i = 1, 2)$:

$$X_3^{*,i} = \frac{S_{3in}^* - S_3^{*,i}}{\alpha_9}$$

Subsequently, $N^{*,i} (i = 1, 2)$ are obtained from the equation (31) as:

$$N^{*,i} = N_{in}^* - \frac{\alpha_{10}}{\alpha_9}(S_{3in}^* - S_3^{*,i})$$

$N^{*,i}$ exist if and only if, $N_{in}^* > \frac{\alpha_{10}}{\alpha_9}(S_{3in}^* - S_3^{*,i})$.

Remark. We denote that:

$$H(S_3) = f(S_3) - g(S_3) = \frac{M(S_3)}{K_{I,nh_3}\alpha_9(S_3^2 + K_{I3}S_3 + K_{I3}K_{S_3})}$$

S_3^* can be, also, deduced from the numerator of $H(S_3)$, denoted $M(S_3)$, and defined by the following third order equation:

$$M(S_3) = a_3 S_3^3 + a_2 S_3^2 + a_1 S_3 + a_0 \tag{32}$$

where

- $a_3 = -D\lambda\alpha_{10}$
- $a_2 = -D(K_{I,nh_3}\alpha_9 + \lambda A\alpha_9 + \lambda\alpha_{10}K_{I3})$
- $a_1 = K_{I3}(K_{I,nh_3}\alpha_9(\bar{\mu}_3 - D) - D\lambda(A\alpha_9 + \alpha_{10}K_{S_3}))$
- $a_0 = -D\alpha_9 K_{S_3}K_{I3}(\lambda A + K_{I,nh_3})$

Using Cardan formulas, $M(S_3)$ is solved explicitly to obtain S_3^*. In this case, no more than two solutions are accepted in view of the constraint of positivity.

Proposition 1.
System (1)-(7) *has at most* 10 *points of equilibrium:*
$E_1 = (\beta_1 S_{in}, \beta_2 S_{in}, 0, 0, 0, 0, N_{in})$, *washout equilibrium, which always exists.*
$E_2 = (\beta_1 S_{in}, S_2^*, S_3^*, 0, X_2^*, 0, N^*)$, *which exists if and only if,* $D < \bar{\mu}_2$.
$E_3^1 = (\beta_1 S_{in}, S_2^*, S_3^{*,1}, 0, X_2^*, X_3^{*,1}, N^{*,1})$, *which exists if and only if,* $D < \bar{\mu}_2$ *and* $X_3^{*,1} > 0$ *and* $\alpha_6 X_2^* > \alpha_9 X_3^{*,1}$ *and* $N_{in} + \alpha_7 X_2^* > \alpha_{10} X_3^{*,1}$.
$E_3^2 = (\beta_1 S_{in}, S_2^*, S_3^{*,2}, 0, X_2^*, X_3^{*,2}, N^{*,2})$, *which exists if and only if,* $D < \bar{\mu}_2$ *and* $X_3^{*,2} > 0$ *and* $\alpha_6 X_2^* > \alpha_9 X_3^{*,2}$ *and* $N_{in} + \alpha_7 X_2^* > \alpha_{10} X_3^{*,2}$.
$E_4 = (S_1^*, \beta_2 S_{in}, S_3^*, X_1^*, 0, 0, N^*)$, *which exists if and only if,* $D < \bar{\mu}_1$ *and* $N_{in} - \alpha_2 X_1^* > 0$.
$E_5^1 = (S_1^*, \beta_2 S_{in}, S_3^{*,1}, X_1^*, 0, X_3^{*,1}, N^{*,1})$, *which exists if and only if,* $D < \bar{\mu}_1$ *and* $X_3^{*,1} > 0$ *and* $\alpha_3 X_1^* > \alpha_9 X_3^{*,1}$ *and* $N_{in} - \alpha_2 X_1^* > \alpha_{10} X_3^{*,1}$.
$E_5^2 = (S_1^*, \beta_2 S_{in}, S_3^{*,2}, X_1^*, 0, X_3^{*,2}, N^{*,2})$, *which exists if and only if,* $D < \bar{\mu}_1$ *and* $X_3^{*,2} > 0$ *and* $\alpha_3 X_1^* > \alpha_9 X_3^{*,2}$ *and* $N_{in} - \alpha_2 X_1^* > \alpha_{10} X_3^{*,2}$.
$E_6 = (S_1^*, S_2^*, S_3^*, X_1^*, X_2^*, 0, N^*)$, *which exists if and only if,* $D < \bar{\mu}_1$ *and* $D < \bar{\mu}_2$ *and* $N_{in} - \alpha_2 X_1^* + \alpha_7 X_2^* > 0$.
$E_7^1 = (S_1^*, S_2^*, S_3^{*,1}, X_1^*, X_2^*, X_3^{*,1}, N^{*,1})$, *which exists if and only if,* $D < \bar{\mu}_1$ *and* $D < \bar{\mu}_2$ *and* $X_3^{*,1} > 0$ *and* $\alpha_3 X_1^* + \alpha_6 X_2^* > \alpha_9 X_3^{*,1}$ *and* $N_{in} - \alpha_2 X_1^* + \alpha_7 X_2^* > \alpha_{10} X_3^{*,1}$.
$E_7^2 = (S_1^*, S_2^*, S_3^{*,2}, X_1^*, X_2^*, X_3^{*,2}, N^{*,2})$, *which exists if and only if,* $D < \bar{\mu}_1$ *and* $D < \bar{\mu}_2$ *and* $X_3^{*,2} > 0$ *and* $\alpha_3 X_1^* + \alpha_6 X_2^* > \alpha_9 X_3^{*,2}$ *and* $N_{in} - \alpha_2 X_1^* + \alpha_7 X_2^* > \alpha_{10} X_3^{*,2}$.

The diagram of Figure 5 summarizes the different cases corresponding to the system equilibria.

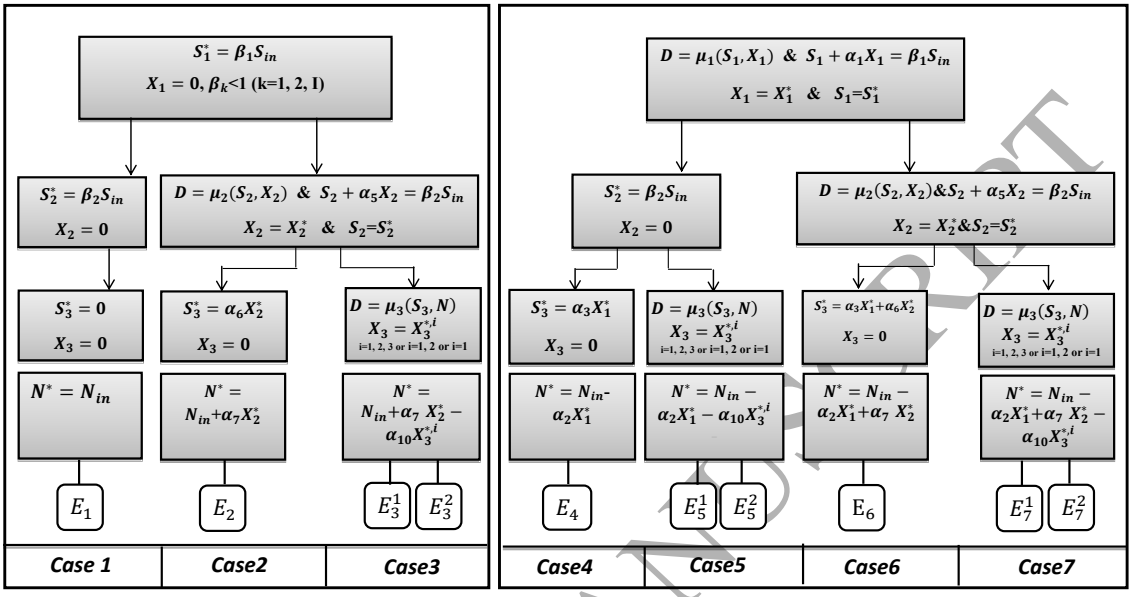

Figure 5: Diagram summarizing the equilibria of system (1)-(7). The system has at most 10 points of equilibrium.

PROOF. See proof in Appendix A.

2.3. Numerical investigation of the stability

The equilibria of the MAD model are dependent on the values of the operating parameters D, S_{in}, N_{in} (Figure 5). Obviously, they greatly affect equilibrium stability and thus the process operation.

To establish whether the equilibria of the MAD model are stable or not, the Jacobian matrix is computed for each equilibrium. If we write the system in the variables $[S_1, X_1, S_2, X_2, S_3, X_3, N]$, the Jacobian matrix will have block-diagonal structure:

$$J = \begin{pmatrix} A & 0_{2*2} & 0_{2*3} \\ 0_{2*2} & B & 0_{2*3} \\ E & F & C \end{pmatrix}$$

In the case where only one or two bacteria at most coexist, the nature of the equilibria can be investigated analytically. The eigenvalues of the Jacobian matrix are those of the matrices A, B and C. We use the Routh-Hurwitz criterion to study the stability

of the matrix C, which is of third-order (see Appendix B).
When all bacterial consortiums coexist, the analytical study of equilibria and their stability becomes very complicated: it is necessary to use numerical tools to find the nature of equilibria. Hereafter, we investigate numerically the equilibria stability with respect to the changes of operating parameters values. Considering a large range of operating parameter values, we construct the operating diagram (see Appendix C) of the MAD model [18, 19].

We fixed the inorganic nitrogen inlet at the average value taken in the experiments $N_{in} = 0.011M$ [16]. Then, for several values of D and S_{in}, we computed equilibria and the corresponding Jacobian matrix. The nature: stability and existence were assigned to each of the 10 equilibria. This enabled us to establish a set of existence-stability combinations for each pair (D, S_{in}) as summarized in Table 3. Each combination is plotted as a colored region $\mathcal{J}_n$ (where n is the number of the combinations) in the operating diagram.
All concentrations are in $(gCOD.L^{-1})$, except the inorganic carbon and the nitrogen which are in (M). The bacterial growth and dilution rates are in (day^{-1}). Nominal values of the model parameters are reported in Table 2.

Table 2: Nominal parameter values used by Mairet et al. [16].

	Parameter			**Unit**
$\beta_1 = 0.3$	$\beta_2 = 0.4$	$\beta_I = 0.3$	$\alpha_1 = 12.5$	$gCOD.gCOD^{-1}$
$\alpha_3 = 11.5$	$\alpha_5 = 9.1$	$\alpha_6 = 8.1$	$\alpha_9 = 20$	
$K_{S_1} = 2.11$	$K_{S_2} = 0.056$			
$\alpha_2 = 0.0062$	$\alpha_4 = 0.03$	$\alpha_7 = 0.054$	$\alpha_8 = 0.03$	$M.gCOD^{-1}$
$\alpha_{10} = 0.0062$	$\alpha_{11} = 0.30$	$\alpha_{12} = 0.20$		
$\bar{\mu}_1 = 0.30$	$\bar{\mu}_2 = 0.053$	$\bar{\mu}_3 = 0.14$	$K_La = 5$	d^{-1}
$K_{S_3} = 0.02$	$K_{I3} = 16.4$			$gCOD.L^{-1}$
$K_C = 4.9e{-}7$	$K_N = 1.1e{-}9$			M
$V_{liq} = 1$	$V_{gas} = 0.1$			L
$K_{H,CO_2} = 2.7e{-}2$				$M.bar^{-1}$
$k_p = 5e4$				$L.d^{-1}.bar^{-1}$
$R = 8.31e{-}2$				$bar.M^{-1}.K^{-1}$
$T_{op} = 308.15$				K

One of the main interests of the operating diagram is to highlight, which equilibria are stable for a given combination of inputs parameters (D, S_{in}).

In order to limit the number of regions plotted in a diagram, we have grouped together the very similar regions, which are just different by the existence of an unstable point. At a neutral pH, it is for instance the case in $\mathcal{J}_4$ where E_3^1 and E_5^1 are unstable if they exist (X in Table 6).

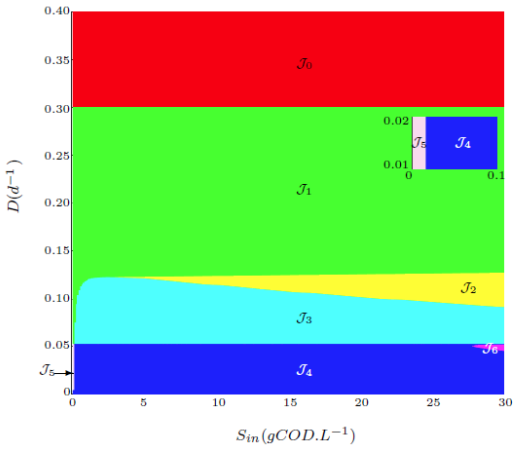

Figure 6: Operating diagram showing the behavior of equilibria as a function of D and S_{in} at $pH = 7$, $N_{in} = 0.011M$. The area $\mathcal{J}_5$ is too small because it exists for only small values of S_{in}.

Table 3: Existence and nature of equilibria according to S_{in} and D at $pH = 7$: Unstable (U), Stable (S), unstable or does not exist (X), Equilibrium does not exist (no sign).

Area	E_1	E_2	E_3^1	E_3^2	E_4	E_5^1	E_5^2	E_6	E_7^1	E_7^2
$\mathcal{J}_0$	S									
$\mathcal{J}_1$	U				S					
$\mathcal{J}_2$	U				S	S	U			
$\mathcal{J}_3$	U				U	S				
$\mathcal{J}_4$	U	U	X		U	X		U	S	
$\mathcal{J}_5$	U	U			U			S		
$\mathcal{J}_6$	U	U	U		U	U		S	S	U

Figure 6 shows seven areas; hence, seven possible combinations of the equilibria can be obtained when pH has a neutral value (see Table 3).
The transition from one region to another, resulting from a change in the model inputs S_{in} and/or D exhibits what is called equilibria bifurcation (appearance, disappearance or coalescence of equilibria). For example, when reading the Figure 6 from the bottom to the top, we notice that an increase of D for a fixed value of $S_{in} = 20gCOD.L^{-1}$ leads to the appearance of several regions: $\mathcal{J}_4$, $\mathcal{J}_3$ and $\mathcal{J}_2$, respectively, evidencing some changes in the nature of the equilibria (as reported in Table 3). When D is very low ($D < 0.04$), we obtain the area ($\mathcal{J}_4$) where only the

functioning equilibrium E_7^1 is stable. A slight increase of D ($0.04 < D < 0.05$) leads to area ($\mathcal{J}_6$): the equilibrium E_6 changes its nature and becomes stable.
An area ($\mathcal{J}_5$) appears when S_{in} is too low and D takes small values ($0.01 < D < 0.05$)(see the zoom, right Figure 6) . In this area the equilibrium E_6 is stable: the consortium X_3 is washed out due to the nitrogen deficiency. If, however, D belongs to the range ($0.05 < D < 0.07$), the system operates in the area ($\mathcal{J}_3$): X_2 is washed out and E_5^1 is stable. An increasing of D with 0.02 d^{-1} leads to area $\mathcal{J}_2$: E_5^1 is still stable, E_4 changes its nature and becomes stable and the stable equilibrium E_5^2 appears. This is due to the bifurcation of the equilibria.

Five of the seven combinations involved one stable equilibrium: E_7^1 ($\mathcal{J}_4$) or E_6 ($\mathcal{J}_5$) when the three reactions occur simultaneously ($D < min(\bar{\mu}_1, \bar{\mu}_2, \bar{\mu}_3)$), E_5^1 ($\mathcal{J}_3$) when D exceeds $\bar{\mu}_2$ (only the reactions (R1) and (R2) take place) and E_4 ($\mathcal{J}_1$) when D is higher than $\bar{\mu}_3$ (only the reaction (R1) take place). When no reaction occurs ($D > max(\bar{\mu}_1, \bar{\mu}_2, \bar{\mu}_3)$), the washout equilibrium E_1 ($\mathcal{J}_0$) becomes stable.
Areas $\mathcal{J}_2$ and $\mathcal{J}_6$ present the bi-stability of the system, where it could tend towards the interior equilibrium or to the washout one, depending on the initial concentration of the methanogens (X_{3_0}). Such operating areas appear when the dilution rate (D) and/or the organic load (S_{in}) reach(es) high levels.

The operating diagram is, then, a good indicator of the risk of AD process failure. It provides good informations about the qualitative properties of the model and the optimum range of operating conditions.
The region $\mathcal{J}_4$ can be defined as a normal operation area, where all the bacteria coexist. It is then the ideal zone to ensure the digester performances.
Areas $\mathcal{J}_5$ and $\mathcal{J}_3$ correspond to the system operation with the washout of X_3 and X_2, respectively. The area $\mathcal{J}_1$ predicts the washout of both X_2 and X_3, and only the consortium X_1 exists. All the bacteria are washed out in the area $\mathcal{J}_0$ that exhibits a high risk of process destabilization .
When the digester operates in the bi-stability areas ($\mathcal{J}_2$, $\mathcal{J}_6$), implementation of a closed-loop regulation system is needed to avoid the washout equilibrium.

2.4. Bifurcation phenomena

In order to highlight the origin of bi-stability, we attempt to show the behaviour of S_3, X_3 and N when Figure 6 is browsed either vertically for a constant organic load or horizontally for a constant dilution rate.
Figure 7 shows the behavior of the existing equilibrium components, capable of changing their nature in accordance with change in the dilution rate.

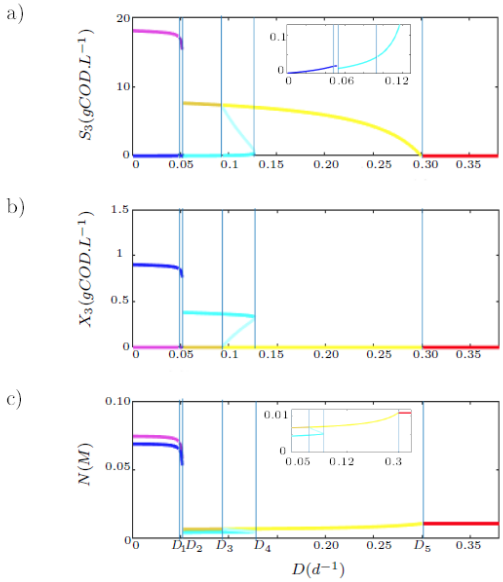

Figure 7: The components of the equilibrium points with respect to the D at $pH = 7$, $S_{in} = 28.5gCOD.L^{-1}$ and $N_{in} = 0.011M$.

E_6 unstable E_7^1 stable E_6 stable E_4 unstable
E_5^1 stable E_4 stable E_1 stable E_5^2unstable

The critical values of D are:

$$D_1 = 0.040, D_2 = \bar{\mu}_2, D_3 = 0.09, D_4 \approx \bar{\mu}_3, D_5 = \bar{\mu}_1$$

with

- $S^*_{3in,total}(D_1) = S_3^{i,*}(D_1)$, with $S_3^{i,*} = \alpha_3 X_1^* + \alpha_6 X_2^* - \alpha_9 X_3^{i,*} (i = 1, 2)$ thus $X_3^{i,*}(D_1) = 0$ (case 7, Figure 5),
- $D_2 = \mu_2(\beta_2 S_{in}, 0)$,
- $S^*_{3in,1}(D_3) = S_3^{i,*}(D_3)$, with $S_3^{i,*} = \alpha_3 X_1^* - \alpha_9 X_3^{i,*} (i = 1, 2)$, thus $X_3^{i,*}(D_3) = 0$ (case 5, Figure 5),
- $D_4 = \mu_3(0, 0)$,

- $D_5 = \mu_1(\beta_1 S_{in}, 0)$.

As can be seen in figure 7, a small change in the dilution rate results in a change of the nature of some model equilibria. For a fixed value of the organic load (S_{in}) increasing D may decrease the concentration of X_3 of the stable equilibrium (Figure 7-b).
It leads to the accumulation of the substrates S_1 and S_2, and then to a considerable production of VFAs (S_3) from reaction 1 (R1) and/or reaction 2 (R2) (see the zoom, top Figure 7-a). This boosts the amount of ionized and non-ionized forms of the VFAs in the reaction medium. Both forms are present with balanced concentrations because the pH is assumed to be neutral. In such case, a potential inhibition of methanogenic bacteria (X_3) occurs by an accumulation of VFAs. Hence, the reaction 3 (R3) will be affected by VFA accumulation: increase of S_3 supported by a significant decrease of X_3.
This risk of inhibition becomes more severe as the organic load (S_{in}) increases. The latter induces high release of ammonia, which explains the appearance of the areas ($\mathcal{J}_2$) and ($\mathcal{J}_6$) where, respectively, the equilibria E_4, E_5^1 and E_6, E_7^1 are stable.
It is clear from Figure 7-c that the nitrogen concentration of the stable equilibria (N^*) is dependent on the value of D. The value of nitrogen at steady-states N^* is higher when D is lower than the maximum growth rate of X_2 ($\bar{\mu}_2$). This is due to the achievement of the reaction (R2) that releases the nitrogen from the breakdown of proteins. This phenomena cannot be observed beyond $\bar{\mu}_2$ because, in this case, the reactor contains only N_{in} as a nitrogen source.
Thus, when $D < \bar{\mu}_2$, the concentration of N^* decreases to satisfy high bacterial needs. However, when $D > \bar{\mu}_2$, bacterial needs decreases because the Hydraulic Retention Time (HRT) is small. Therefore, nitrogen consumption is not high and N^* concentration increases (see the zoom, top Figure 7-c).
This reveals that increasing D may increase the risk of process failure by providing an excess of S_3, not an excess of nitrogen (because D alleviates the ammonia stress [11]).
Figures 8 and 9 present the behavior of the components of existing equilibria, capable to change their nature when the organic load (S_{in}) varies, and D is lower and higher than $\bar{\mu}_2$, respectively.

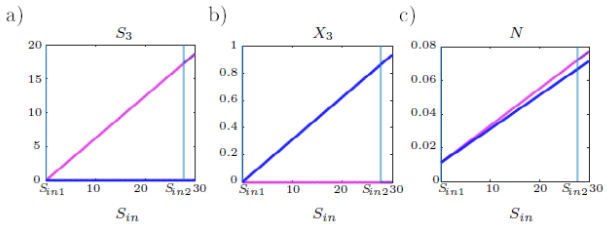

Figure 8: The components of the equilibrium points with respect to S_{in} at $pH = 7$, $D = 0.0301d^{-1}$ and $N_{in} = 0.011M$.

The critical values of the organic load S_{in1} and S_{in2} are around $0.02gCOD.L^{-1}$ and $28.5gCOD.L^{-1}$, respectively, with:

$$S^*_{3in,total}(S_{in1}) > S^{i,*}_3(S_{in1}), \text{thus} \quad X^{i,*}_3(S_{in1}) > 0 \quad \text{(case 7, Figure 5)}.$$

$$S^*_{3in,total}(S_{in2}) = S^{i,*}_3(S_{in2}), \text{thus} \quad X^{i,*}_3(S_{in2}) = 0 \quad \text{(case 7, Figure 5)}.$$

For a fixed value of $D < \bar{\mu}_2$, the increase of the organic load yields high concentrations of the substrates S_1 and S_2 in the medium. The concentrations of the bacteria and inorganic nitrogen N^* of the stable equilibria (E_6 before S_{in1}, E^1_7 before S_{in2} and E_6/E^1_7 after exceeding S_{in2}) increase accordingly. This can be regarded as abnormal behavior because no inhibition is seen even though the ammonia concentration is high and VFAs have accumulated.

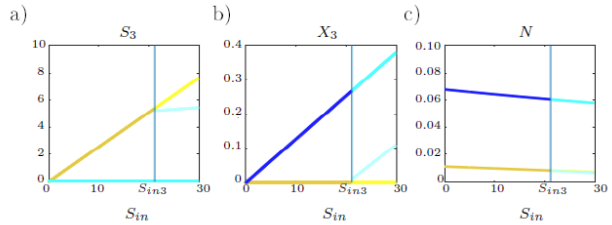

Figure 9: The components of the equilibrium points with respect to S_{in} at $pH = 7$, $D = 0.101d^{-1}$ and $N_{in} = 0.011M$.

If D is fixed at a constant value beyond $\bar{\mu}_2$ (X_2 washed out), the critical value of the organic load is about $S_{in3} = 21.5\ gCOD.L^{-1}$, with:

$$S^*_{3in,1}(S_{in3}) = S^{i,*}_3(S_{in3}), \text{thus} \quad X^{i,*}_3(S_{in3}) = 0 \quad \text{(case 5, Figure 5)}.$$

The increase of S_{in} leads to an increase of S_3 and a decrease of N of the stable equilibria (E_5^1 before S_{in_3} and E_4/E_5^1 after exceeding S_{in_3}). Consequently, X_3 increases by consuming S_3 and the nitrogen coming from N_{in}.
These results show that a small change to the control parameters may lead to a noteworthy change in the MAD behavior. Special attention must be given to their values to avoid process failure.

3. Global behavior of the system

3.1. Influence of pH

It is well known that pH plays a key role in Anaerobic Digestion. It can, thus, cause the imbalance of ions at certain values.
pH may suddenly rise during the treatment of protein materials rich in nitrogen, particularly at low buffer capacity. At high levels, pH promotes the release of unionized ammonia toxic to methanogens, while at low levels, free acids formation is significant and bacteria are inhibited by VFAs accumulation.
Simulation and experimental results presented in Mairet el al. [16] stress that the pH can vary between 6.5 and 7.5 throughout the digestion of *chlorella vulgaris* microalgae.
To emphasize pH influence on the AD of such protein-rich substrates, we establish below the operating diagram of the MAD model in an acidic medium (pH = 6.5) as well as in a basic medium (pH = 7.5). In the following simulations, the representation of the operating diagram is made with D ranging from 0 to 0.15.

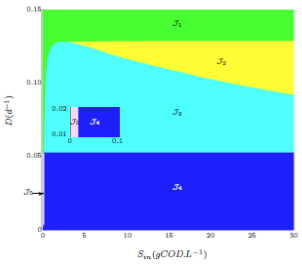

Figure 10: Operating diagram - behavior of equilibria as a function of varying D and S_{in} at $pH = 6.5$, $N_{in} = 0.011M$. The area $\mathcal{J}_5$ is too small in the OD because it exists for only small values of S_{in}.

Table 4: Existence of equilibria and stability at $pH = 6.5$, $N_{in} = 0.011M$: unstable (U), stable (S), unstable or does not exist (X), equilibrium does not exist (no sign).

Area	E_1	E_2	E_3^1	E_3^2	E_4	E_5^1	E_5^2	E_6	E_7^1	E_7^2
$\mathcal{J}_0$	S									
$\mathcal{J}_1$	U				S					
$\mathcal{J}_2$	U				S	S	U			
$\mathcal{J}_3$	U				U	S				
$\mathcal{J}_4$	U	U	X		U	X		U	S	
$\mathcal{J}_5$	U	U			U			S		

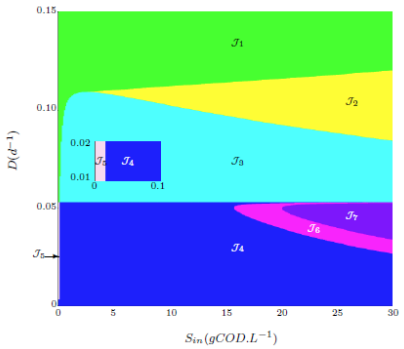

Figure 11: Operating diagram - behavior of equilibria as a function of varying D and S_{in} at $pH = 7.5$, $N_{in} = 0.011M$. The area $\mathcal{J}_5$ is too small in the OD because it exists for only small values of S_{in}.

Table 5: Existence of equilibria and stability at $pH = 7.5$: unstable (U), stable (S), unstable or does not exist (X), equilibrium does not exist (no sign).

Area	E_1	E_2	E_3^1	E_3^2	E_4	E_5^1	E_5^2	E_6	E_7^1	E_7^2
$\mathcal{J}_0$	S									
$\mathcal{J}_1$	U				S					
$\mathcal{J}_2$	U				S	S	U			
$\mathcal{J}_3$	U				U	S				
$\mathcal{J}_4$	U	U	X		U	X		U	S	
$\mathcal{J}_5$	U	U			U			S		
$\mathcal{J}_6$	U	U	U		U	U		S	S	U
$\mathcal{J}_7$	U	U	U	U	U	U		S	S	U

By comparing the operating diagrams representing an acidic pH (Figure 10) and a neutral pH (Figure 6), we find the same areas except for $\mathcal{J}_6$, a bi-stability area undesirable from a practical point of view. Moreover, when the pH takes a neutral value, we can see that the bi-stability area $\mathcal{J}_2$ appears at a dilution value that causes a total washout of X_3.
The risk of process failure at $pH = 7$ seems to be higher than that observed at $pH = 6.5$. Such a result does not agree with the numerous studies in the literature that prove the sensitivity of methanogens to high VFAs concentrations [20, 21]. Henceforth, the value chosen for the inhibition constant K_{I3} associated to VFA (S_3) and proposed in Mairet et al. prevents the occurrence of an inhibition by an excess of VFAs. We have plotted in Figure 12 the pattern of methanogens growth rate for a small value of K_{I3}.

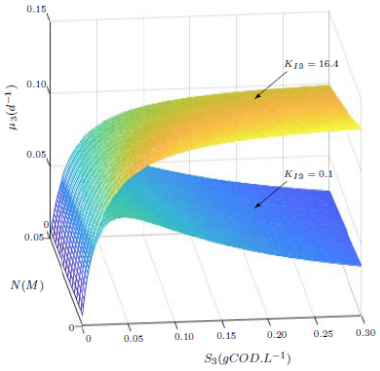

Figure 12: Methanogen growth rates

From Figure 12, it is clear that the X_3 growth rate with the K_{I3} value reported in Mairet et al. [16] exhibits a Monod-like behavior. The inhibition of growth is only observed if smaller value of K_{I3} are used (Haldane function). This confirms our assumption and points out a significant limitation of the MAD model.

The comparison of Figure 11 with Figure 6 highlights new area $\mathcal{J}_7$ in a basic reaction medium, Figure 11 shows that the areas $\mathcal{J}_4$ and $\mathcal{J}_3$ narrow and the bi-stability zones are wider.

Indeed, when $D < \bar{\mu}_2$, the increase of S_{in} leads to bi-stability ($\mathcal{J}_6$ to $\mathcal{J}_7$). This is due to the continuous increase in the amount of nitrogen produced from (R2) and promoted by the pH. When D exceeds $\bar{\mu}_2$, this risk is halved because (R2) is no longer active. In summary, the higher the organic load, the greater amount of nitrogen in the medium. In particular, at a pH of 7.5, there is a shift leading to a higher Free Ammonia production, increasing the risk of process failure.

3.2. Biogas yield

The biogas flow rate is defined in Mairet et al. [16] by the equation (15). At equilibrium, biogas flow rate can be written as:

$$q^*_{gas} = k_p(P^*_{CH_4} + P^*_{CO_2} - P_{atm}) \tag{33}$$

$P^*_{CO_2}$ and $P^*_{CH_4}$ can be deduced by setting the right-hand sides of equations (8), (9) and (10) equal to zero. From the first equation, we can define C^* depending on the model inputs and outputs:

$$C^{*i} = C_{in} + \alpha_4 X^*_1 + \alpha_8 X^*_2 + \alpha_{12} X^{*i}_3 - \frac{\rho_{CO2}}{D} \tag{34}$$

By replacing (13), (14) and (33) in the equations (9) and (10), we get the following subsystem of two equations:

$$\begin{cases} -k_p P_{CO_2}^2 - P_{CO_2}(k_p P_{CH_4} - k_p P_{atm} + k_L a K_{H,CO_2} V_{liq} RT_{op}) + \frac{h}{K_C+h} k_L a V_{liq} ... \\ ... RT_{op} C^*(X_1^*, X_2^*, X_3^*, P_{CO_2}, P_{CH_4}) = 0 \\ -k_p P_{CH_4}^2 - k_p P_{CH_4}(P_{CO_2} - P_{atm}) + \alpha_{11}\mu_3 X_3^{*i} V_{liq} RT_{op} = 0 \end{cases} \tag{35}$$

Solutions of (35) allows the calculation of the biogas flow rate at equilibrium (Figure 13).

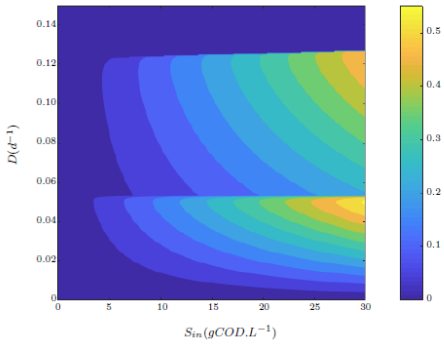

Figure 13: Biogas flow rate as a function of (D, S_{in}) changes at $pH = 7$, $N_{in} = 0.011M$.

Biogas yield shown in Figure 13 is highly dependent on the values of control parameters. For a fixed value of nitrogen inlet concentration N_{in}, optimum biogas production is obtained for a dilution rate lower than the maximum growth rate $\bar{\mu}_2$. Moreover, a significant enhancement of biogas yield takes place when S_{in} is high (yellow zone). It matches the area in which all bacteria coexist ($\mathcal{J}_4$ and $\mathcal{J}_6$). The maximum production is, then, obtained when the equilibria E_7^1 and E_6 are stable.
However, when D is greater than $\bar{\mu}_2$ ($\mathcal{J}_3$) less production of biogas is observed. Similarly, the highest yield is reached in the bi-stability area (E_5^1 and E_4) when we operate around the interior equilibrium.
Otherwise, no biogas production is observed beyond the area $\mathcal{J}_3$ due to the washout of methanogen bacteria.
Hence, we must focus on a suitable choice of X_{3_0} in the area of bi-stability in order to avoid the inhibition of bacteria on the one hand and, to ensure the maximum production of biogas on the other.

3.3. Relationship between S_{in}, D and N_{in}

In addition to S_{in}, the inlet concentration of the inorganic nitrogen N_{in} may constitute a potential source of nitrogen in the reaction medium. The deficiency or excess of Nitrogen limits the development of microorganisms by preventing/inhibiting bacterial growth and causing an imbalance in their intracellular pH. This leads to the process failure.

To get more insight into its influence, we evaluate its relationship with the concentration of the organic load. In simulations, we study the maximum tolerated value of N_{in} that guarantees process stability, for the predefined range of S_{in} ($0 < S_{in} < 30$) and the optimum value of the dilution rate ($D = 0.05\ d^{-1}$).
We establish the operating diagram as a function of changes in S_{in} and N_{in} (Figure 14).

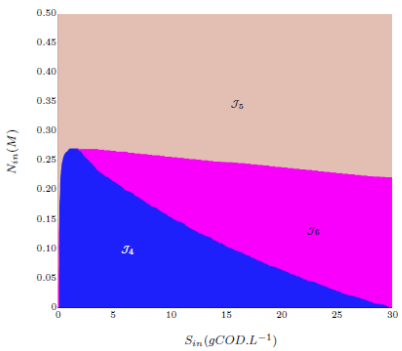

Figure 14: Operating diagram with respect to N_{in} and S_{in} with $D = 0.05d^{-1}$.

Table 6: Possible areas when N_{in} and S_{in} vary at $pH = 7$, $D = 0.05\ d^{-1}$: unstable (U), stable (S), unstable or does not exist (X), equilibrium does not exist (no sign).

Area	E_1	E_2	E_3^1	E_3^2	E_4	E_5^1	E_5^2	E_6	E_7^1	E_7^2
$\mathcal{J}_4$	U	U	X		X	X		U	S	
$\mathcal{J}_5$	U	U			U	X	X	S		
$\mathcal{J}_6$	U	U	X	X	U	X	X	S	S	U

It is clear from Figure 14 that increasing both N_{in} and S_{in} leads to bi-stability ($\mathcal{J}_6$), and possibly the washout of microorganisms ($\mathcal{J}_5$), due to the severe risk of

the ammonia toxicity. Bistability or washout can, also, take place in presence of the small concentrations of S_{in} and N_{in} in the reactor. Thus, the optimal concentration of N_{in} belongs to the area ($\mathcal{J}_4$). It maximum value is highly dependent on the organic load: its decreases when S_{in} increases.
Indeed, when S_{in} reaches its maximum value and N_{in} is too small the process operate in the bi-stability area ($\mathcal{J}_6$) where both the equilibria E_6 and E_7^1 are stable. However, in the case of low concentration of S_{in} and high nitrogen inlet value, the bacteria are washed out ($\mathcal{J}_5$) and only the equilibrium E_6 is stable. The washout of methanogens is due to an excess of nitrogen in the reaction medium: released from the breakdown of proteins, in the first case, and derived from the nitrogen input concentration, in the second case.
Nitrogen input has a significant influence on model behavior. A sudden rise in its value might lead to process failure even if D and S_{in} belong to their optimal ranges.

4. Discussion

4.1. Operating parameters acting on ammonia toxicity

Our study highlights the qualitative properties of a model treating the digestion of a protein-rich substrate at a mesophilic temperature of 35 ^oC. The mathematical analysis of the model allows us to emphasize the control parameters affecting process performances. The major parameters acting on ammonia toxicity are: the organic load (S_{in}), the nitrogen input concentration (N_{in}) and the dilution rate (D). An increase of the first two parameters favors a large amount of nitrogen that can lead to bi-stability. Under such conditions, a slight variation in X_{3_0} concentration may cause process failure (Figure 6). When the pH reaches a basic level, these bi-stabilities occur even with a small value of S_{in} ($\mathcal{J}_6$, $\mathcal{J}_7$) due to the buffering capacity of the reaction medium (Figure 11). However, regardless of the system pH, values of S_{in} and N_{in} that are too low cause the bacterial washout by nitrogen deficiency.
The changes of the previous parameters greatly affect bacterial communities (Table 3), in particular the methanogen consortia that acts directly on biogas yield. They can be limited either by a low nitrogen concentration, or inhibited by high ammonia release or still by a large amount of VFAs in the reactor.
At a neutral pH, using the operating diagram (Figure 6), we established that the desirable area for ideal operation of process is the area $\mathcal{J}_4$ where no bacterial consortia were washed out. A comparison of Figures 6 and 10 with the Figure 11 reveals that the optimum value for the pH is 7. Thus, to guarantee process stability, the operator must keep the bioreactor inputs within the ranges D $[0.001 - 0.05]d^{-1}$,

S_{in} $[0.03 - 28] gCOD.L^{-1}$, at a neutral pH. In addition, Figure 13 shows that the optimum yield of the MAD model in terms of biogas production was obtained for the following ranges $[0.001 - 0.05] d^{-1}$, $[0.03 - 30] gCOD.L^{-1}$ of S_{in} and D, respectively. This was the case, when D was close to $\bar{\mu}_2$. The maximum value of biogas production is then reached in the area of the bi-stability ($\mathcal{J}_6$) where small changes to the methanogen concentration may lead to washout (boundary equilibrium E_6). In this case, particular attention must be paid to the X_{3_0} concentration as well as the dilution rate value because any change on this latter can inhibit X_2 and so alter process functioning in rendering E_5^1 stable.
Figure 14 shows the relationship between the concentrations of S_{in} and N_{in} when D takes its optimal value for biogas production ($D = 0.05\ d^{-1}$).
To ensure process stability ($\mathcal{J}_4$), the ideal concentration of nitrogen inlet (N_{in}) should be chosen according to the value of S_{in}. In presence of a rising concentration of the organic load, N_{in} value must be the smallest possible to satisfy the bacterial needs, on the one hand, and to avoid the threshold level of inhibition, on the other hand.

4.2. MAD model limitations

It is well known that an acidic medium in an AD bioreactor favors the formation of free VFAs, inhibitors of methanogenic bacteria. Notice however that no inhibition occured when we plotted the OD at $pH = 6.5$ (Figure 10). This means that the MAD model is not able to predict realistic process behavior at low pH. It is a limitation of the model, which it is actually due to the fact that in the study of Mairet et al. [16], the Haldane inhibition constant ($K_{I_3} = 16.4\ gCOD.L^{-1}$) was too large. Bernard et al. [22] and Benyahia et al. [23] have assumed that the value of this parameter is around 256 $mmol.L^{-1}$ and 40 $mmol.L^{-1}$ (Table1 of [23]), which matches 0.2713 $gCOD.L^{-1}$ and 0.058 $gCOD.L^{-1}$, respectively.

To check the impact of a small value of K_{I3} parameter on process behavior, we simulated the operating diagram of the model with an intermediate value of K_{I3}, about 0.1 $gCOD.L^{-1}$.

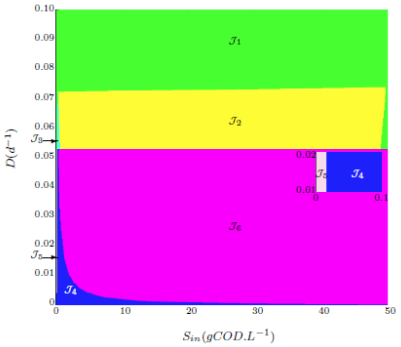

Figure 15: Operating diagram showing equilibria behavior as a function of D and S_{in} at $pH = 6.5$, $N_{in} = 0.011M$, $K_{I3} = 0.1$. The area $\mathcal{J}_5$ is too small in the OD because it appears for only small values of S_{in}.

Table 7: Existence and nature of equilibria as a function of S_{in} and D at $pH = 6.5$, $N_{in} = 0.011M$, $K_{I3} = 0.1$: unstable (U), stable (S), unstable or does not exist (X), equilibria does not exist (no sign).

Area	E_1	E_2	E_3^1	E_3^2	E_4	E_5^1	E_5^2	E_6	E_7^1	E_7^2
$\mathcal{J}_1$	U				S					
$\mathcal{J}_2$	U				S	S	U			
$\mathcal{J}_3$	U				U	S				
$\mathcal{J}_4$	U	U	U		U	U		U	S	
$\mathcal{J}_5$	U	U			U	X	X	S		
$\mathcal{J}_6$	U	U	X	X	U	X	X	S	S	U

Figure 15 shows that, at an acidic pH, the MAD model becomes more sensitive to high VFAs concentrations with this value of K_{I3}. The appropriate operational region for process operation ($\mathcal{J}_4$) narrows and the instability is reached at a value of D and S_{in} ensuring the stability while $K_{I3} = 16.4\ gCOD.L^{-1}$. This parameter plays a significant role when the process operates at a low pH where the formation of un-ionized VFAs is considerable.

5. Properties of the ADM1m model in view of the properties of MAD model

Mairet et al. [16] showed that the MAD model presents the same dynamic behavior as a modified ADM1 model [17]: ADM1 adapted to the AD of microalgae, called hereafter ADM1m. Investigating the qualitative properties of such a complex model give a general insight into process behavior, useful in the case of operation and control of the production of biogas.
These properties can be investigated either by simulations requiring powerful numerical tools [24], or by the study of a reduced ADM1m model. Based on the equivalence of the ADM1m model and the MAD model, we try, to investigate the qualitative and quantitative properties of the ADM1m model using the findings on the MAD model properties presented above.

5.1. Qualitative properties of the ADM1m model

From the OD of the MAD model (Figure 6) we can observe that, for a fixed value of $S_{in} = 2\ gCOD.L^{-1}$, the progressive increase of D leads to the emergence of areas $\mathcal{J}_4$, $\mathcal{J}_3$, $\mathcal{J}_1$, $\mathcal{J}_0$.
The transition from the operational zone $\mathcal{J}_4$ to $\mathcal{J}_3$, $\mathcal{J}_1$ and $\mathcal{J}_0$ involves, respectively, the washout of the bacteria X_2, X_3 and X_1. The total washout of microorganisms is then indicated by the area $\mathcal{J}_0$, obtained for large values of the dilution rate. However, we can see from the same figure that small values of S_{in} induce bacterial washout by nitrogen while, higher values of S_{in} led to bi-stability, even to washout area when K_{I3} is too low (Figure 15).
Thus, the washout can be caused either by a high dilution rate, a low organic load or by an organic overload.

Compared to the original ADM1, the simulations of the ADM1m model show a shift in the amount of various intermediate products, mainly the inorganic nitrogen concentration [17]. This is due to the different hydrolysis kinetics considered by the two models: a first-order kinetic and a Contois kinetic are assigned for the first and second models, respectively. Fekih-Salem et al. [25] demonstrate that, in the case of the 'Anaerobic digestion models', the change in the hydrolysis rate may act only on the amount of soluble organic matter. It assumes, then, that the qualitative properties are not affected.

Hence, to verify our results and enhance scope of their validity, we tried to compare the qualitative properties of the ADM1m model with those of the orginal ADM1 numerically studied by Bornhöft et al. [24]. The authors stressed that the washout of the ADM1 model can occur either by: i) an increase in the dilution rate; ii) a

decrease of substrate concentration (due to famine); or iii) an increase of input substrate concentration (leading to inhibition).
All these properties of the ADM1 model correspond very well to the properties of the ADM1m model [24].

5.2. Quantitative properties of the ADM1m model

As well as qualitative properties, quantitative properties of the ADM1m model can also be revealed from the equilibria calculation of the MAD model. Khedim et al. [26], established equivalence relationships between the MAD and ADM1m models using the states-variables association method proposed in [27]. These relations are simple algebraic equations where each variable of the MAD model is defined as a combination of variables of the ADM1m model (Table 8).

Table 8: States-Variables association ADM1m-MAD [26].

MAD variables	Associated ADM1 variables
S_1 (g COD/l)	$S_{su} + S_{fa} + X_c + X_{ch} + X_{li}$
S_2 (g COD/l)	$S_{aa} + X_{pr}$
S_3 (g COD/l)	$S_{va} + S_{bu} + S_{pro} + S_{ac}$
X_1 (g COD/l)	$X_{su} + X_{fa}$
X_2 (g COD/l)	X_{aa}
X_3 (g COD/l)	$X_{c4} + X_{pro} + X_{ac} + X_{h2}$
N (M)	S_{in}
C (M)	S_{ic}
z (M)	$S_{Cat} - S_{An}$
P_{CO2} (bar)	$P_{gas,co2}$
P_{CH4} (bar)	$P_{gas,ch4}$
S_I $(gCOD/l)$	$S_i + X_I$
q_{gas} (Ld^{-1})	q_{gas}

Based on these combinations, we have evaluated the equilibrium value of the MAD and ADM1m models.
We apply the same dilution rates and organic loads to both models. Then, for each value of D and S_{in}, we calculate the value of the stable equilibrium in the corresponding area. In the case of bi-stability ($\mathcal{J}_6$ or $\mathcal{J}_2$), we represent the interior point (positive equilibrium excluding washout). Calculation results are reported in Table 9.

Table 9 shows a good correspondence between the equilibrium values of the MAD

Table 9: Equilibria values of ADM1m-MAD models in each area.

Area	models	Dilution rate / organic load values	S_1	S_2	S_3	X_1	X_2	X_3	N
$\mathcal{J}_0$	ADM1m	$D = 0.35$, $S_{in} = 15$	4.1602	6.1747	0	0	0	0	0.0109
	MAD		4.5	6	0	0	0	0	0.0110
$\mathcal{J}_1$	ADM1m	$D = 0.2$, $S_{in} = 15$	2.4625	6.2185	0.3642	0.1494	0	0.0718	0.0095
	MAD		1.1435	6	3.08	0.2685	0	0	0.0093
$\mathcal{J}_2$	ADM1m	$D = 0.12$, $S_{in} = 28$	1.4806	11.6867	0.1591	0.4376	0	0.2947	0.0061
	MAD		0.8545	11.2000	0.1653	0.6036	0	0.3388	0.0051
$\mathcal{J}_3$	ADM1m	$D = 0.07$, $S_{in} = 15$	0.3526	6.3002	0.0866	0.2341	0	0.1600	0.0082
	MAD		0.2211	6	0.0217	0.3423	0	0.1957	0.0076
$\mathcal{J}_4$	ADM1m	$D = 0.025$, $S_{in} = 15$	0.1574	0.1523	0.0553	0.1807	0.2843	0.4081	0.0479
	MAD		0.0684	0.0328	0.0057	0.3545	0.6557	0.4691	0.0413
$\mathcal{J}_6$	ADM1m	$D = 0.0491$, $S_{in} = 29.5$	0.4144	1.1963	0.1161	0.4432	0.6503	0.9537	0.0759
	MAD		0.2845	0.8315	0.0191	0.6852	1.205	0.8812	0.0663

model and those of the ADM1m model. Slight differences between the values of some variables may be due to the fact that bacterial death is not accounted for the MAD model.

However, a significant offset in the VFA concentration can be observed in most regions. These gaps in the results can be explained by the fact that the MAD model considers only the acetic acid while the modified ADM1 model takes into account also the propionic, valeric, butyric, acetic acids. The high value of the Haldane inhibition constant K_{I3} considered in the MAD model can also be another cause of such mismatches. These results validate, on one hand, the theoretical results obtained by the mathematical study of the MAD model and stress its ability - with a modified Haldane inhibition constant - to predict the behavior of a more complex model such as the ADM1m model.

Thus, ADM1m can be controlled via the study of the MAD model, which appears to be a good candidate for synthesizing control laws.

6. Conclusion

This paper presents the mathematical analysis of a Microalgae Anaerobic Digestion (MAD) model. The qualitative properties of the model were compared with those of the original and modified ADM1 models. Simulation results show the key role of control parameters in process behavior as well as the strong effect of pH on the digestion of protein-rich substrates. On the one hand, these results enable us to identify the ideal conditions for the operation of such digestion. On the other, they give an insight into the behavior of the modified ADM1 solutions. Thus, they should be very helpful for controlling AD processes treating protein-rich substrates.

Perspectives of this work include the extension of the present results to the case where the pH is not constant, stressing the qualitative properties of the model in such cases. This will be useful for knowing how to proceed under the different pHs of the system as well as for a wide range of organic load and dilution rates.

Appendix A. Proof of proposition 1

PROOF. An equilibrium point $\xi^* = (S_1^*, S_2^*, S_3^*, X_1^*, X_2^*, X_3^*, N^*)$ of the system must be a solution of (19a-19g) with the left-hand side equal to zero. From equation (19d), we have:

- $X_1^* = 0$; hence, using (19a), one obtains $S_1^* = \beta_1 S_{in}$
- or S_1^* and X_1^* must satisfy equation $\mu_1(S_1, X_1) = D$; hence, using (19a), one gets S_1^* and X_1^* together as a solution of (20a-20b). Therefore S_1^* and X_1^* are given by (25) and (24), respectively.

Similarly, from equation (19e) it is deduced that:

- $X_2^* = 0$; hence, using (19b), one obtains $S_2^* = \beta_2 S_{in}$
- or S_2^* and X_2^* must satisfy equation $\mu_2(S_2, X_2) = D$; hence, using (19b), one obtains S_2^* and X_2^* as a solution of (21a-21b). Therefore, S_2^* and X_2^* are given by (28) and (27), respectively.

On the other hand, from equation (19f) it is deduced that:

- $X_3^* = 0$; hence, using (19c) and (19g), one obtains S_3^* and N^* with respect of S_1^*, X_1^*, S_2^* and X_2^*
- or S_3^* and N^* must satisfy equation $\mu_3(S_3, N) = D$; hence, using (19c) and (19g), one obtains S_3^*, X_3^* and N^* as a solution of (22a-22c). Therefore, X_3^* and N^* are given by (29) and (30), respectively, where S_3^* is a solution of equation (32) satisfying the condition $S_3^* < S_{3in}^*$.
  Eight cases must be distinguished, as shown in Table 1. The 8th case corresponding to $X_1 = 0$, $X_2 = 0$, $X_3 \neq 0$ cannot occur since, according to (19f), we would have $\mu_3 = D$ and hence, using (19c) we will obtain

$$DS_3^* + \alpha_9 X_3^* = 0$$

  which is impossible (positivity property of biological systems is not fulfilled). The rest of the proof is illustrated in Figure 5.

Appendix B. Analytical calculation of equilibria nature (*c.f* 2.3)

When we consider $\xi = [S_1, X_1, S_2, X_2, S_3, X_3, N]^T$, the state vector of the model MAD, the Jacobian matrix will be described as a block-diagonal structure:

$$J = \begin{pmatrix} A & 0_{2*2} & 0_{2*3} \\ 0_{2*2} & B & 0_{2*3} \\ E & F & C \end{pmatrix}$$

where

$$A = \begin{pmatrix} -D - \alpha_1 X_1 \mu'_{1S} & -X_1\alpha_1\mu'_{1X} - \alpha_1\mu_1(S_1^*, X_1^*) \\ X_1\mu'_{1S} & \mu_1(S_1^*, X_1^*) - D + X_1\mu'_{1X} \end{pmatrix},$$

$$B = \begin{pmatrix} -D - \alpha_5 X_2 \mu'_{2S} & -X_2\alpha_5\mu'_{2X} - \alpha_5\mu_2(S_2^*, X_2^*) \\ X_2\mu'_{2S} & \mu_2(S_2^*, X_2^*) - D + X_2\mu'_{2X} \end{pmatrix},$$

$$E = \begin{pmatrix} \alpha_3 X_1 \mu'_{1S} & \alpha_3 X_1\mu'_{1X} + \alpha_3\mu_1(S_1^*, X_1^*) \\ 0 & 0 \\ -\alpha_2 X_1 \mu'_{1S} & -\alpha_2\mu_1(S_1^*, X_1^*) - \alpha_2 X_1\mu'_{1X} \end{pmatrix},$$

$$F = \begin{pmatrix} \alpha_6 X_2 \mu'_{2S} & \alpha_6 X_2\mu'_{2X} + \alpha_6\mu_2(S_2^*, X_2^*) \\ 0 & 0 \\ \alpha_7 X_2 \mu'_{2S} & \alpha_7\mu_2(S_2^*, X_2^*) + \alpha_7 X_2\mu'_{2X} \end{pmatrix},$$

$$C = \begin{pmatrix} C11 & C12 & C13 \\ C21 & C22 & C23 \\ C31 & C32 & C33 \end{pmatrix}.$$

with

$$\begin{array}{lll} C11 = -D - \alpha_9 X_3 \mu'_{3S} & , \quad C12 = -\alpha_9\mu_3 & , \quad C13 = -\alpha_9 X_3\mu'_{3N} \\ C21 = X_3\mu'_{3S} & , \quad C22 = -D + \mu_3 & , \quad C23 = X_3\mu'_{3N} \\ C31 = -\alpha_{10} X_3\mu'_{3S} & , \quad C32 = -\alpha_{10}\mu_3 & , \quad C33 = -D - X_3\alpha_{10}\mu'_{3N} \end{array}$$

and

$$\mu'_{1S} = \frac{\partial\mu_1(S_1^*, X_1^*)}{\partial S_1}, \quad \mu'_{1X} = \frac{\partial\mu_1(S_1^*, X_1^*)}{\partial X_1}, \quad \mu'_{2S} = \frac{\partial\mu_2(S_2^*, X_2^*)}{\partial S_2},$$

$$\mu'_{2X} = \frac{\partial \mu_2(S_2^*, X_2^*)}{\partial X_2}, \quad \mu'_{3S} = \frac{\partial \mu_3(S_3^*, N^*)}{\partial S_3}, \quad \mu'_{3N} = \frac{\partial \mu_3(S_3^*, N^*)}{\partial N}$$

The eigenvalues of the Jacobian matrix are the eigenvalues of matrices A, B and C. Since A and B are square matrices, we can calculate their trace and determinant. To guarantee the system stability: traces must be negatives (*tr(matrix)<0*) and determinants must be positives (*det(matrix)>0*).
The stability of the matrix C can be tested using the Routh-Hurwitz criterion, in particular in the case of the equilibria E_5^i and E_7^i. For example

- The calculation of Jacobian matrix at the equilibrium E_1 gives:

$$A = \begin{pmatrix} -D & -a_1\mu_1(\beta_1 S_{in}, 0) \\ 0 & \mu_1(\beta_1 S_{in}, 0) - D \end{pmatrix},$$

$$B = \begin{pmatrix} -D & -a_5\mu_2(\beta_2 S_{in}, 0) \\ 0 & \mu_2(\beta_2 S_{in}, 0) - D \end{pmatrix},$$

$$C = \begin{pmatrix} -D & -\alpha_9\mu_3(0, N_{in}) & 0 \\ 0 & -D + \mu_3(0, N_{in}) & 0 \\ 0 & -a10\mu_3(0, N_{in}) & -D \end{pmatrix}.$$

The eigenvalues of A and B are negative (*i.e.* $tr(A) < 0, tr(B) < 0$) and ($det(A) > 0$, $det(B) > 0$) if, and only if, $\mu_1(\beta_1 S_{in}, 0) < D$, $\mu_2(\beta_2 S_{in}, 0) < D$, respectively.

Since the matrix C is block-triangular, its eigenvalues are $-D$ and the eigenvalues of the second order matrix in the upper left corner. Since, this second order matrix is an upper triangular matrix, its eigenvalues are on the diagonal, *i.e.* $-D$ and $-D+\mu_3(0, N_{in})$. Thus, C is stable if, and only if, $\mu_3(0, N_{in}) < D$. The stability of the matrix C can also be investigated using the Routh-Hurwitz criterion where the characteristic polynomial is defined by:

$$P_{E_1} = \Lambda^3 + (-\mu_3(0, N_{in}) + 3D)\Lambda^2 + (3D^2 - 2D\mu_3(0, N_{in}))\Lambda - D^2\mu_3(0, N_{in}) + D^3$$

Thus, the Routh array is

Λ^3	1	$3D^2 - 2D\mu_3(0, N_{in})$	0
Λ^2	$-\mu_3(0, N_{in}) + 3D$	$-D^2\mu_3(0, N_{in}) + D^3$	0
Λ^1	cst1	0	0
Λ^0	cst2	0	0

with

$$\begin{aligned} cst1 &= \frac{1}{-\mu_3(0,N_{in})+3D}[(-\mu_3(0,N_{in})+3D)(3D^2-2D\mu_3(0,N_{in})) - (-\mu_3(0,N_{in}) \\ & D^2+D^3)] \\ cst2 &= -D^2\mu_3(0,N_{in})+D^3 \end{aligned}$$

The Routh-Hurwitz criterion require that all the terms of the first column of array must have the same sign. Since the first term of the first column is positive then all the subsequent terms must be positive, *i.e.* $-\mu_3(0,N_{in})+3D$, $cst1$ and $cst2$, to fullfill the stability condition. It yields that the necessar condition to garantee that the eigenvalues of the matrix C are negative is $\mu_3(0,N_{in}) < D$. Hence, if $S_1^* < \beta_1 S_{in}$, $S_2^* < \beta_2 S_{in}$ and $S_3^{*,i} < S_{3in}^*$, the equilibrium E_1 is locally asymptotically stable. This equilibrium is unstable if $S_1^* > \beta_1 S_{in}$, $S_2^* > \beta_2 S_{in}$ or $S_3^{*,i} > S_{3in}^*$.

- The assessment of the Jacobian matrix around the equilibrium E_4 gives:

$$A = \begin{pmatrix} -D-a_1X_1^*\mu_{1S}^{'} & -a_1X_1^*\mu_{1X}^{'}-a_1D \\ \mu_{1S}^{'}X_1^* & \mu_{1X}^{'}X_1^* \end{pmatrix},$$

$$B = \begin{pmatrix} -D & -a_5\mu_2(\beta_2 S_{in},0) \\ 0 & \mu_2(\beta_2 S_{in},0)-D \end{pmatrix},$$

$$C = \begin{pmatrix} -D & -\alpha_9\mu_3(S_{3in,1}^*,N_{in,1}^*) & 0 \\ 0 & \mu_3(S_{3in,1}^*,N_{in,1}^*)-D & 0 \\ 0 & -\alpha_{10}\mu_3(S_{3in,1}^*,N_{in,1}^*) & -D \end{pmatrix}.$$

The eigenvalues of the matrix B has a negative real part if, and only if, $\mu_2(\beta_2 S_{in},0) < D$. We obtain for matrix A :

$$tr(A) = -D - \alpha_1 X_1^*\mu_{1S}^{'} + \mu_{1X}^{'}X_1^*$$

$$det(A) = DX_1^*(-\mu_{1X}^{'} + \alpha_1\mu_{1S}^{'})$$

The eigenvalues of the matrix A are negatives if, and only if,

$$\alpha_1\mu_{1S}^{'} > \mu_{1X}^{'}$$

In this case, the characteristic polynomial of the matrix C is:

$$P_{E_4} = \Lambda^3 + (3D - \mu_3(S^*_{3in,1}, N^*_{in,1}))\Lambda^2 + (3D^2 - 2D\mu_3(S^*_{3in,1}, N^*_{in,1})\Lambda + D^2(D - \mu_3(S^*_{3in,1}, N^*_{in,1}))$$

Using the Routh-Hurwitz criterion, we can deduce that the matrix C is stable if, and only if, $\mu_3(S^*_{3in,1}, N^*_{in,1}) < D$. This can also be deduced easily from the structure of the matrix C whose eigenvalues are simply the values on the diagonal, *i. e.* $-D$, $\mu_3(S^*_{3in,1}, N^*_{in,1}) - D$ and $-D$. The matrix is stable if, and only if, $\mu_3(S^*_{3in,1}, N^*_{in,1}) < D$.

- We obtain from calculation of the Jacobian matrix around the equilibria E^i_5 $(i = 1, 2)$, the following submatrices:

$$A = \begin{pmatrix} -D - a_1 X^*_1 \mu'_{1S} & -a_1 X^*_1 \mu'_{1X} - a_1 D \\ \mu'_{1S} X^*_1 & \mu'_{1X} X^*_1 \end{pmatrix},$$

$$B = \begin{pmatrix} -D & -a_5 \mu_2(\beta_2 S_{in}, 0) \\ 0 & \mu_2(\beta_2 S_{in}, 0) - D \end{pmatrix},$$

$$C = \begin{pmatrix} C11_{E^i_5} & C12_{E^i_5} & C13_{E^i_5} \\ C21_{E^i_5} & C22_{E^i_5} & C23_{E^i_5} \\ C31_{E^i_5} & C32_{E^i_5} & C33_{E^i_5} \end{pmatrix}.$$

with

$$\begin{aligned} C11_{E^i_5} &= -D - (S^*_{3in,1} - S^*_3)\mu'_{3S} \\ C12_{E^i_5} &= -\alpha_9 D \\ C13_{E^i_5} &= -(S^*_{3in,1} - S^*_3)\mu'_{3N} \\ C21_{E^i_5} &= \frac{(S^*_{3in,1} - S^*_3)}{\alpha_9}\mu'_{3S} \\ C22_{E^i_5} &= 0 \\ C23_{E^i_5} &= \frac{(S^*_{3in,1} - S^*_3)}{\alpha_9}\mu'_{3N} \end{aligned}$$

$$
\begin{aligned}
C31_{E_5^i} &= -a_{10}\frac{(S^*_{3in,1}-S^*_3)}{\alpha_9}\mu^{'}_{3S}\\
C32_{E_5^i} &= -\alpha_{10}D\\
C33_{E_5^i} &= -D-a_{10}\frac{(S^*_{3in,1}-S^*_3)}{\alpha_9}\mu^{'}_{3N}
\end{aligned}
$$

The eigenvalues of the matrix B have a negative real part if, and only if, $\mu_2(\beta_2 S_{in},0)<D$. We obtain for matrix A:

$$tr(A) = -D-\alpha_1 X_1^*\mu^{'}_{1S}+\mu^{'}_{1X}X_1^*$$

$$det(A) = DX_1^*(-\mu^{'}_{1X}+\alpha_1\mu^{'}_{1S})$$

The eigenvalues of A are negatives if, and only if,

$$\alpha_1\mu^{'}_{1S} > \mu^{'}_{1X}$$

However, the stability of matrix C can be checked using the Routh-Hurwitz criterion, where the characteristic polynomial is:

$$
\begin{aligned}
P_{E_5^i} =&\Lambda^3+\frac{1}{\alpha_9}(2\alpha_9 D+\alpha_{10}\mu^{'}_{3N}S^*_{3in}-\alpha_{10}\mu^{'}_{3N}S^*_3-\alpha_9\mu^{'}_{3S}S^*_3+\alpha_9\mu^{'}_{3S}S^*_{3in})\Lambda^2+\frac{1}{\alpha_9}\\
&(2DS^*_{3in}\alpha_{10}\mu^{'}_{3N}-2S^*_3\alpha_{10}D\mu^{'}_{3N}+2\mu^{'}_{3S}DS^*_{3in}\alpha_9-2\mu^{'}_{3S}S^*_3\alpha_9 D+\alpha_9 D^2)\Lambda+\\
&\frac{1}{\alpha_9}(\mu^{'}_{3S}D^2S^*_{3in}\alpha_9-\mu^{'}_{3N}\alpha_{10}D^2S^*_3-\mu^{'}_{3S}D^2S^*_3\alpha_9+\mu^{'}_{3N}\alpha_{10}D^2S^*_{3in})
\end{aligned}
$$

The stability is guaranteed when all the coefficients of the first column of Routh matrix retain the same sign. In this case, the conditions of stability can't be easily deduced.

- The calculation of Jacobian matrix at the equilibrium E_6, gives:

$$
A=\begin{pmatrix} -D-\alpha_1 X_1^*\mu^{'}_{1S} & -\alpha_1 X_1^*\mu^{'}_{1X}-\alpha_1 D\\ \mu^{'}_{1S}X_1^* & \mu^{'}_{1X}X_1^*\end{pmatrix},
$$

$$
B=\begin{pmatrix} -D-\alpha_5 X_2^*\mu^{'}_{2S} & -\alpha_5 X_2^*\mu^{'}_{2X}-\alpha_5 D\\ \mu^{'}_{2S}X_2^* & \mu^{'}_{2X}X_2^*\end{pmatrix},
$$

$$
C=\begin{pmatrix} -D & -\alpha_9\mu_3(S^*_{3in,total},N^*) & 0\\ 0 & \mu_3(S^*_{3in,total},N^*)-D & 0\\ 0 & -\alpha_{10}\mu_3(S^*_{3in,total},N^*) & -D\end{pmatrix}.
$$

We obtain for matrix A

$$tr(A) = -D - \alpha_1 X_1^* \mu_{1S}^{'} + \mu_{1X}^{'} X_1^*$$

$$det(A) = DX_1^*(-\mu_{1X}^{'} + \alpha_1 \mu_{1S}^{'})$$

The eigenvalues of the matrix A are negative if, and only if,

$$\alpha_1 \mu_{1S}^{'} > \mu_{1X}^{'}$$

We have for matrix B

$$tr(B) = -D - \alpha_5 X_2^* \mu_{2S}^{'} + \mu_{2X}^{'} X_2^*$$

$$det(B) = X_2^* D(-\mu_{2X}^{'} + \alpha_5 \mu_{2S}^{'})$$

The eigenvalues of the matrix B are negative if, and only if,

$$\alpha_5 \mu_{2S}^{'} > \mu_{2X}^{'}$$

The characteristic polynomial of matrix C is:

$$P_{E_6} = \Lambda^3 + (3D - \mu_3(S_{3in,total}^*, N^*))\Lambda^2 + (3D^2 - 2D\mu_3(S_{3in,total}^*, N^*))\Lambda + D^2 (D - \mu_3(S_{3in,total}^*, N^*))$$

Using the Routh-Hurwitz criterion, we can deduce that the matrix C is stable if, and only if, $D > \mu_3(S_{3in,total}^*, N^*)$. This condition guarantees that all the coefficients of the first column of Routh table retain the same sign. This can also be deduced evidently from the block-triangular form of the matrix C

- The Jacobian matrix calculation around the equilibria E_7^i $(i = 1, 2)$, gives:

$$A = \begin{pmatrix} -D - \alpha_1 X_1^* \mu_{1S}^{'} & -\alpha_1 X_1^* \mu_{1X}^{'} - \alpha_1 D \\ \mu_{1S}^{'} X_1^* & \mu_{1X}^{'} X_1^* \end{pmatrix},$$

$$B = \begin{pmatrix} -D - \alpha_5 X_2^* \mu_{2S}^{'} & -\alpha_5 X_2^* \mu_{2X}^{'} - \alpha_5 D \\ \mu_{2S}^{'} X_2^* & \mu_{2X}^{'} X_2^* \end{pmatrix},$$

$$C = \begin{pmatrix} C11_{E_7^i} & C12_{E_7^i} & C13_{E_7^i} \\ C21_{E_7^i} & C22_{E_7^i} & C23_{E_7^i} \\ C31_{E_7^i} & C32_{E_7^i} & C33_{E_7^i} \end{pmatrix}.$$

with

$$
\begin{aligned}
C11_{E_7^i} &= -D - (S^*_{3in,total} - S^*_3)\mu^{'}_{3S} \\
C12_{E_7^i} &= -\alpha_9 D \\
C13_{E_7^i} &= -(S^*_{3in,total} - S^*_3)\mu^{'}_{3N} \\
C21_{E_7^i} &= \frac{\mu^{'}_{3S}(S^*_{3in,total} - S^*_3)}{\alpha_9} \\
C22_{E_7^i} &= 0 \\
C23_{E_7^i} &= \frac{\mu^{'}_{3N}(S^*_{3in,total} - S^*_3)}{\alpha_9} \\
C31_{E_7^i} &= -\frac{\alpha_{10}(S^*_{3in,total} - S^*_3)\mu^{'}_{3S}}{\alpha_9} \\
C32_{E_7^i} &= -\alpha_{10} D \\
C33_{E_7^i} &= -D - \frac{\alpha_{10}(S^*_{3in,total} - S^*_3)\mu^{'}_{3N}}{\alpha_9}
\end{aligned}
$$

For matrix A, we have

$$tr(A) = -D - \alpha_1 X_1^* \mu^{'}_{1S} + \mu^{'}_{1X} X_1^*$$

$$det(A) = D X_1^* (-\mu^{'}_{1X} + \alpha_1 \mu^{'}_{1S})$$

The eigenvalues of the matrix A are negative if, and only if,

$$\alpha_1 \mu^{'}_{1S} > \mu^{'}_{1X}$$

For matrix B, we obtain

$$tr(B) = -D - \alpha_5 X_2^* \mu^{'}_{2S} + \mu^{'}_{2X} X_2^*$$

$$det(B) = X_2^* D(-\mu_{2X} + \alpha_5 \mu_{2S})$$

The eigenvalues of the matrix B are negative if, and only if,

$$\alpha_5 \mu^{'}_{2S} > \mu^{'}_{2X}$$

As in the case of equilibrium E_5^i, the conditions of stability of the matrix C obtained at the equilibria E_7^i cannot be easily deduced using the Routh-Hurwitz criterion in view of the complicated form of the characteristic polynomial presented as below:

Table B1: Analytical study of the stability of MAD equilibria.

Equilibria	Area	D, S_{in}	Trace of matrices	Determinant of matrices	Routh-Hurwitz criterion/condition of existence	nature of equilibrium
E_1	$\mathcal{J}_0$	$D = 0.35$	$tr(A) < 0$	$det(A) > 0$	all the coefficients of the first Routh column> 0	E_1 stable
		$S_{in} = 6$	$tr(B) < 0$	$det(B) > 0$		
	$\mathcal{J}_1$	$D = 0.20$	$tr(A) < 0$	$det(A) < 0$	all the coefficients of the first Routh column> 0	E_1 unstable
		$S_{in} = 6$	$tr(B) < 0$	$det(B) > 0$		
	$\mathcal{J}_2$	$D = 0.1$	$tr(A) > 0$	$det(A) < 0$	all the coefficients of the first Routh column> 0	E_1 unstable
		$S_{in} = 25$	$tr(B) < 0$	$det(B) > 0$		
	$\mathcal{J}_3$	$D = 0.07$	$tr(A) > 0$	$det(A) < 0$	all the coefficients of the first Routh column> 0	E_1 unstable
		$S_{in} = 6$	$tr(B) < 0$	$det(B) > 0$		
	$\mathcal{J}_4$	$D = 0.03$	$tr(A) > 0$	$det(A) < 0$	all the coefficients of the first Routh column> 0	E_1 unstable
		$S_{in} = 6$	$tr(B) < 0$	$det(B) < 0$		
	$\mathcal{J}_5$	$D = 0.04$	$tr(A) > 0$	$det(A) < 0$	all the coefficients of the first Routh column> 0	E_1 unstable
		$S_{in} = 0.01$	$tr(B) < 0$	$det(B) < 0$		
	$\mathcal{J}_6$	$D = 0.04$	$tr(A) > 0$	$det(A) < 0$	all the coefficients of the first Routh column> 0	E_1 unstable
		$S_{in} = 29$	$tr(B) < 0$	$det(B) < 0$		
E_4	$\mathcal{J}_1$	$D = 0.15$	$tr(A) < 0$	$det(A) > 0$	all the coefficients of the first Routh column> 0	E_4 stable
		$S_{in} = 6$	$tr(B) < 0$	$det(B) > 0$		
	$\mathcal{J}_2$	$D = 0.1$	$tr(A) < 0$	$det(A) > 0$	all the coefficients of the first Routh column> 0,	E_4 stable
		$S_{in} = 25$	$tr(B) < 0$	$det(B) > 0$		
	$\mathcal{J}_3$	$D = 0.07$	$tr(A) < 0$	$det(A) > 0$	not all the coefficients of the first Routh column> 0	E_4 unstable
		$S_{in} = 6$	$tr(B) < 0$	$det(B) > 0$		
	$\mathcal{J}_4$	$D = 0.03$	$tr(A) < 0$	$det(A) > 0$	not all the coefficients of the first Routh column> 0	E_4 unstable
		$S_{in} = 6$	$tr(B) < 0$	$det(B) < 0$		
	$\mathcal{J}_5$	$D = 0.04$	$tr(A) < 0$	$det(A) > 0$	all the coefficients of the first Routh column> 0	E_4 unstable
		$S_{in} = 0.01$	$tr(B) < 0$	$det(B) < 0$		
	$\mathcal{J}_6$	$D = 0.04$	$tr(A) < 0$	$det(A) > 0$	not all the coefficients of the first Routh column> 0	E_4 unstable
		$S_{in} = 29$	$tr(B) > 0$	$det(B) < 0$		
E_5^1	$\mathcal{J}_2$	$D = 0.1$	$tr(A) < 0$	$det(A) > 0$	all the coefficients of the first Routh column> 0	E_5^1 stable
		$S_{in} = 25$	$tr(B) < 0$	$det(B) > 0$		
	$\mathcal{J}_3$	$D = 0.07$	$tr(A) < 0$	$det(A) > 0$	all the coefficients of the first Routh column> 0	E_5^1 stable
		$S_{in} = 6$	$tr(B) < 0$	$det(B) > 0$		
	$\mathcal{J}_4$	$D = 0.03$	$tr(A) < 0$	$det(A) > 0$	all the coefficients of the first Routh column> 0	E_5^1 unstable
		$S_{in} = 6$	$tr(B) < 0$	$det(B) < 0$		
	$\mathcal{J}_6$	$D = 0.04$	$tr(A) < 0$	$det(A) > 0$	all the coefficients of the first Routh column> 0	E_5^1 unstable
		$S_{in} = 29$	$tr(B) < 0$	$det(B) < 0$		
E_6	$\mathcal{J}_4$	$D = 0.03$	$tr(A) < 0$	$det(A) > 0$	not all the coefficients of the first Routh column> 0	E_6 unstable
		$S_{in} = 6$	$tr(B) < 0$	$det(B) > 0$		
	$\mathcal{J}_5$	$D = 0.04$	$tr(A) < 0$	$det(A) > 0$	all the coefficients of the first Routh column> 0	E_6 stable
		$S_{in} = 0.01$	$tr(B) < 0$	$det(B) > 0$		
E_7^1	$\mathcal{J}_4$	$D = 0.03$	$tr(A) < 0$	$det(A) > 0$	all the coefficients of the first Routh column> 0	E_7^1 stable
		$S_{in} = 6$	$tr(B) < 0$	$det(B) > 0$		
	$\mathcal{J}_6$	$D = 0.04$	$tr(A) < 0$	$det(A) > 0$	all the coefficients of the first Routh column> 0	E_7^1 stable
		$S_{in} = 29$	$tr(B) < 0$	$det(B) > 0$		

$$P_{E_7^i} = \Lambda^3 + \frac{1}{\alpha_9}(\mu'_{3S}S^*_{3in}\alpha_9 - \mu'_{3S}S^*_3\alpha_9 - \alpha_{10}S^*_3\mu'_{3N} + 2\alpha_9 D + \alpha_{10}\mu'_{3N}S^*_{3in})\Lambda^2 + \frac{1}{\alpha_9}(2D$$
$$\mu'_{3S}S^*_{3in}\alpha_9 + 2S^*_{3in}\alpha_{10}D\mu'_{3N} - 2S^*_3\alpha_{10}D\mu'_{3N} + \alpha_9 D^2 - 2S^*_3\alpha_9\mu'_{3S}D)\Lambda + \frac{1}{\alpha_9}(D^2\mu'_{3N}$$
$$\alpha_{10}S^*_{3in} - S^*_3\alpha_{10}D^2\mu'_{3N} + S^*_{3in}\alpha_9 D^2\mu'_{3S} - \mu'_{3S}D^2\alpha_9 S^*_3)$$

Notice that the Jacobian matrix was not evaluated around the equilibria E_2 and E_3^i because they have never been stable (see Tables 3, 4, 5).

Application

The stability of Jacobian matrix is investigated for some values of D and S_{in}, using the previous analytical calculations as illustrated in Table B1.

Appendix C. Algorithm of the Operating Diagram

The operating diagram is the two-parameter bifurcation scheme that shows how the system behaves when we vary two control parameters [28].
Due to the higher order of the MAD model, the system's behavior with respect to the changes of D, S_{in} and N_{in} cannot be investigated analytically. Hence, we obtain the operating diagram of the MAD model using numerical simulations realized with MATLAB.
Initially the script performs a calculation of the eigenvalues of the Jacobian matrix defined for the MAD model. These calculations are evaluated for each equilibrium of the MAD around certain values of D and S_{in}. According to the sign of the eigenvalues and the conditions of existence, we assign to each of 10 equilibria: stability, instability or non existence. This procedure gives a set of combinations matching pairs of values (D, S_{in}).

Algorithm 1 Operating diagram.

Model input
for i varying from 1 to length (D) **do**
  for j varying from 1 to length (S_{in}) **do**
    calculate values of the 10 equilibria of the model $E = E_1$, ..., E_7^2
    for k varying from 1 to length (E) **do**
      calculate the Jacobian matrix around E_k (J_{E_k})
      calculate the eigenvalues of (J_{E_k})
      if all (the conditions of existence of E_k are fulfilled & all the eigenvalues of (J_{E_k}) are non-positive) **then**
        E_k is stable
      else if all (conditions of existence of E_k are fulfilled & any of the eigenvalues of (J_{E_k}) is positive) **then**
        E_k is unstable
      else
        E_k does not exist
      end if
    end for
  end for
end for

Acknowledgements

Authors thank the Hubert Curien Tassili project 15MDU949 and the Euro-Mediterranean TREASURE Research Network (cf. www.inra.fr/treasure) for their financial support. Authors also thank Jean-Philippe Steyer, Francis Mairet and Olivier Bernard for fruitful discussions about this work.

References

References

[1] U. Baserga, Co-digestion in agricultural biogas plants. Digestion of organic residues and energy grass for biogas production, J. Food and Agriculture Organization of the United Nation. 512 (1998).

[2] E. Kovács, R. Wirth, G. Maróti, Z. Bagi, K. Nagy, J. Minárovits, G. Rákhely, K.L. Kovács, Augmented biogas production from protein-rich substrates and associated metagenomic changes, J. Bioresource Technology. 178 (2015) 254-261.

[3] O. Yenigün, B. Demirel, Ammonia inhibition in anaerobic digestion: A review, J. Process Biochemistry. 48 (2013) 901-911.

[4] F. Lü, M. Chen, P-J. He, L-M. Shao, Effects of Ammonia on Acidogenesis of Protein-Rich Organic Wastes, J. Environmental Engineering Science. 25 (2008) 114-122.

[5] F. Omil, R. Méndez, J.M. Lema, Anaerobic treatment of saline wastewater under high sulphide and ammonia content, J. Bioresource Technology. 54 (1995) 268-278.

[6] L. Guerrero, F. Omil, R. Méndez, J.M. Lema, Anaerobic hydrolysis and acidogenesis of wastewaters from food industries with high content of organic solids and protein, J. Water Research. 33 (1999) 3281-3290.

[7] L. Zhang, D. Jahng, Long-term anaerobic digestion of food waste stabilized by trace elements, J. Waste Management. 32 (2012) 1509-1515.

[8] C. Resch, A. Wörl, R. Waltenberger, R. Braun, R. Kirchmayr, Enhancement options for the utilisation of nitrogen rich animal by-products in anaerobic digestion, J. Bioresource Technology. 102 (2011) 2503-2510.

[9] B. Zhang, L. Zhang, S. Zhang, H. Shi, W. Cai, The influence of pH on hydrolysis and acidogenesis of kitchen wastes in two-phase anaerobic digestion, J. Environ. Technol. 26 (2005) 329-340.

[10] M. Ortner, K. Leitzinger, S. Skupien, G. Bochmann, W. Fuchs, Efficient anaerobic mono-digestion of N-rich slaughterhouse waste: influence of ammonia, temperature and trace elements, J. Bioresour. Technol. 174 (2014) 222-232.

[11] A. Hejnfelt, I. Angelidaki, Anaerobic digestion of slaughterhouse by-products, J. Biomass. Bioenergy. 33 (2009) 1046-1054.

[12] A.O. Wagner, P. Lins, C. Malin, C. Reitschuler, P. Illmer, Impact of protein-, lipid- and cellulose-containing complex substrates on biogas Production and microbial communities in batch experiment, J. Science of the Total Environment. 458-460, 256-266 (2013).

[13] D.J. Batstone, J. Keller, R.B. Newell, M. Newland, Modelling anaerobic degradation of complex wastewater. I: model development, J. Bioresource Technology. 75 (2013) 67-74.

[14] LY. Lokshina, V. Vavilin, E. Salminen, J. Rintala, Modeling of anaerobic degradation of solid slaughterhouse waste: inhibition effects of long-chain fatty acids or ammonia, J. Appl. Biochem. Biotechnol. 109 (2003) 15-32.

[15] I. Angelidaki, B. K. Ahring, Methods for increasing the biogas potential from the recalcitrant organic matter contained in manure In: Mata-Alvarez, J., Tilche, A., Cecchi, F. (Eds.), Proceedings of the Second International Symposium on Anaerobic Digestion of Solid Wastes, Barcelona, 1999.

[16] F. Mairet, O. Bernard, E. Cameron, M. Ras, L. Lardon, J-P. Steyer, B. Chachuat, Three-Reaction Model for the Anaerobic Digestion of Microalgae, J. Biotechnology and Bioengineering. 109 (2011) 415-429.

[17] F. Mairet, O. Bernard, M. Ras, L. Lardon, J-P. Steyer, Modeling anaerobic digestion of microalgae using ADM1, J. Bioresource Technology. 102 (2011) 6823-6829.

[18] M.J. Wade, J. Oakley, S. Harbisher, N.G. Parker, J. Dolfing, MI-Sim: A MATLAB package for the numerical analysis of microbial ecological interactions, J. Public Library of Science (PLoS ONE). 12 (2017) 1-15.

[19] M.J. Wade, R.W. Pattinson, N.G. Parker, J. Dolfing, Emergent behaviour in a chlorophenol-mineralising three-tiered microbial 'food web', J. Theoretical Biology. 389 (2016) 171-186.

[20] B. K. Ahring, M. Sandberg, I. Angelidaki, Volatile fatty acids as indicators of process imbalance in anaerobic digestors, J. Appl. Microbiol. Biotechnol. 43 (1994) 559-565.

[21] D.J. Batstone, J. Keller, I. Angelidaki, S.V. Kalyuzhnyi, S.G. Pavlostathis, A. Rozzi, W.T. Sanders, H. Siegrist, V.A. Vavilin, Anaerobic digestion Model No.1(ADM1), J. Water. Sci. Techno. 45 (2002) 65-73.

[22] O. Bernard, Z. Hadj-Sadock, D. Dochain, A. Genovesi, J-P. Steyer, Dynamical Model Development and Parameter Identification for an Anaerobic Wastewater Treatment Process, J. Biotechnologie and Bioengineering. 75 (2001) 424-438.

[23] B. Benyahia, T. Sari, B. Cherki, J. Harmand, Bifurcation and stability analysis of a two step model for monitoring anaerobic digestion processes, J. Process Control. 22 (2012) 1008-1019.

[24] A. Bornhöft, R. Hanke-Rauschenbach, K. Sundmacher, Steady-state analysis of the Anaerobic Digestion Model No. 1 (ADM1), J. Nonlinear Dynamics. 73 (2013) 535-549.

[25] R. Fekih-Salem, N. Abdellatif, T. Sari, J. Harmand, Analyse mathématique d'un modèle de digestion anaérobie à trois étapes, J. ARIMA. 17 (2014) 53-71.

[26] Z. Khedim, B. Benyahia, F. Mairet, J-P. Steyer, J. Harmand, Reduction of a complex biotechnological process model using state-variable association method-Application to the anaerobic digestion of micro-algae, Proceedings of the 2017 International Conference on Control, Automation and Diagnosis, Hammamet, 2017.

[27] S. Hassam, E. Ficara, A. Leva, J. Harmand, A generic and systematic procedure to derive a simplified model from the Anaerobic Digestion Model No.1 (ADM1), J. Biochemical Engineering. 99 (2015) 193-203.

[28] T. Sari, M. J. Wade, Generalised approach to modelling a three-tiered microbial food-web, J. Mathematical Biosciences. 291 (2017) 21-37.